A STRUCTURAL STUDY OF

Li_xMO_2 (M = Ru, Ir and Os)

A STRUCTURAL STUDY OF THE LITHIUM INTERCALATES OF RuO_2, IrO_2 and OsO_2

By

ISOBEL JEAN DAVIDSON, B.Sc.

A Thesis

Submitted to the School of Graduate Studies

in Partial Fulfilment of the Requirements

for the Degree

Master of Science

McMaster University

May 1983

MASTER OF SCIENCE (1983) McMASTER UNIVERSITY

(Chemistry) Hamilton, Ontario

TITLE: A Structural Study of the Lithium Intercalates of RuO_2, IrO_2 and OsO_2

AUTHOR: Isobel Jean Davidson, B.Sc. (McMaster University)

SUPERVISOR: Professor J.E. Greedan

NUMBER OF PAGES: viii, 84

ABSTRACT

The insertion of lithium into the rutile structures RuO_2 and IrO_2 was found, by X-ray powder diffraction, to result in the formation of the orthorhombic phases $Li_{0.9}RuO_2$ and $Li_{0.9}IrO_2$, respectively. The orthorhombic cells of the intercalation products are related to the tetragonal transition metal dioxide cells by a large expansion ($\sim$ 0.5 Å) in the [100] and [010] directions and a smaller contraction ($\sim$ 0.3 Å for $Li_{0.9}RuO_2$ and 0.05 Å for $Li_{0.9}IrO_2$) along the [100] axis. Both Li_xRuO_2 and Li_xIrO_2 are two phased systems over the range of lithium compositions studied ($0.2 \lesssim x \lesssim 0.9$).

The structure of $Li_{0.9}RuO_2$ was determined by neutron powder diffraction. The structure adopted by $Li_{0.9}RuO_2$ is a distorted NiAs-type structure quite similar to that of a related compound $LiMoO_2$. Unresolved difficulties were encountered in attempting to prepare samples of Li_xOsO_2 and Li_xIrO_2 suitable for their structure determination.

ACKNOWLEDGEMENTS

It is my great pleasure to acknowledge the contributions of my supervisor, J.E. Greedan to the completion of this work. His encouragement and guidance were indispensable. The able technical assistance of J.D. Garrett, H.F. Gibbs and J. Couper is greatly appreciated. I would also like to thank S. Eicher, J.P. Goral and C. Turner for many helpful discussions, and K. Lushington for his generous help with different aspects of this project and for granting me liberal access to his computer. The assistance of M. Ashraf in editing the manuscript and drafting the diagrams is gratefully acknowledged. The encouragement and support of my collegues in room 440 has been essential to the completion of this project. I am especially grateful to Kerstin Stockman for her excellent typing of the manuscript in a very short time.

TABLE OF CONTENTS

LIST OF FIGURES

LIST OF TABLES

CHAPTER 1

INTRODUCTION

Li_xMO_2 (M = Ru, Os and Ir) are members of a class of materials known as intercalation compounds. Members of this group, particularly those involving lithium, have good prospects for application as cathode materials in high energy density, secondary (or rechargable) batteries. Proposed applications for these batteries include vehicle propulsion, off-peak electrical energy storage, and self-contained power supplies for small electronic devices (Murphy and Christian 1979). Lithium, being the lightest and most electropositive metal, is an unusually attractive anode material, and in cases where the free energy of reaction between lithium and the cathode material is large, the system offers the possibility of a high energy density. Greater understanding of the physical properties and reaction mechanism of known intercalation compounds may indicate modifications which will make these compounds more useful as cell materials or suggest new applications.

Intercalation is a topochemical reaction in which the insertion of a "guest" species into a "host" lattice is accompanied by only minimal changes in the host structure (Thomas 1974). In the ideal case of no change in the host

structure, the transition states of the forward and reverse reaction are similar and consequently, the reaction is reversible. Therefore, when the intercalation reaction is of the redox type, the product of the reaction may be useful as a cathode in a secondary electrochemical cell.

Techniques developed for topochemical insertion of lithium have been reviewed by Whittingham (1978); only those methods mentioned in this work will be discussed here. A simple and mild technique for intercalating lithium involves the use of n-butyl lithium (Dines 1975). To lithiate the host compound, it is simply immersed in an approximately 0.2 M solution of n-butyl lithium in hexane at ambient temperature for about a week under an inert atmosphere. The major co-product of the reaction is octane formed from the two butyl radicals:

$$C_4H_9Li + TiS_2 \rightarrow LiTiS_2 + \tfrac{1}{2}C_8H_{18}.$$

The composition of the product is controlled by the quantity of lithium present in the solution, but if only partial lithiation is desired, time must be allowed for equilibration between particles because the reaction is not reversible (Whittingham 1978).

Electrochemical methods in which the host material serves as the cathode and lithium metal as the anode have also been successful in preparing intercalation compounds; for example, $Li_xV_6O_{13}$ can be prepared from the cell:

Li/1 M $LiAsF_6$ in propylene carbonate/V_6O_{13} (Murphy et al 1979). These reactions proceed spontaneously under the chemical concentration gradient, and the composition of the product can be controlled by monitoring the total current passed or by regulating the cell potential. This electrochemical cell may be veiwed as a rechargable battery in which intercalation represents the discharging of the cell. Lithium can be removed from the product simply by applying a reverse potential; this is equivalent to charging the cell.

The essential requirements for an intercalation product to be a good cathode material (Whittingham 1978), are that it has:

i) a large free energy of formation to produce a high cell voltage,

ii) a wide range of composition with little change in free energy over the range to permit high cell capacities,

iii) little structural change on reaction to comply with the reversibility requirement, and

iv) high diffusivity to yield a high power density.

Other desirable properties (Murphy and Christian 1979) are good electrical conductivity and low solubility in the electrolyte to minimize resistive heat generation and to prevent self-discharge respectively.

The materials most likely to fulfill these requirements are those that have layered structures or vacant channels, a high free energy of formation, an accessible and unfilled

electronic band structure, and transition metal ions in their higher oxidation states (Whittingham 1978). The class of lithium intercalation compounds which have been studied the most intensely are the two-dimensional, Van der Waals bonded structures such as the transition metal dichalcogenides. In these materials the Van der Waals gap between the layers widens to accommodate the lithium, thus providing enough vacant sites to permit a wide range of composition and to facilitate lithium ion diffusion (Murphy and Christian 1979).

Many three-dimensional materials exist with vacant channel sites approximately large enough for lithium ion insertion. A prime example of these are the rutile-related transition metal dioxides. The variation in properties provided by this class of compounds should enable the determination of the importance of channel size, electronic conductivity and structural distortions to reversible lithium intercalation. Most of the previous work on these compounds has been done by a group in Bell Labs (Murphy et al 1978). They reported that a number of transition metal dioxides having rutile-related structures rapidly and reversibly incorporate lithium, with greater quantities of lithium being inserted when the host cell has a volume greater than 62 $\mathring{A}^3$ and is metallic (Fig. 1.1). It was suggested that the metallic conductivity might aid lithium insertion through the screening of the Coulombic repulsion between the lithium ions by the conduction electrons (Murphy et al 1978). However, metallic

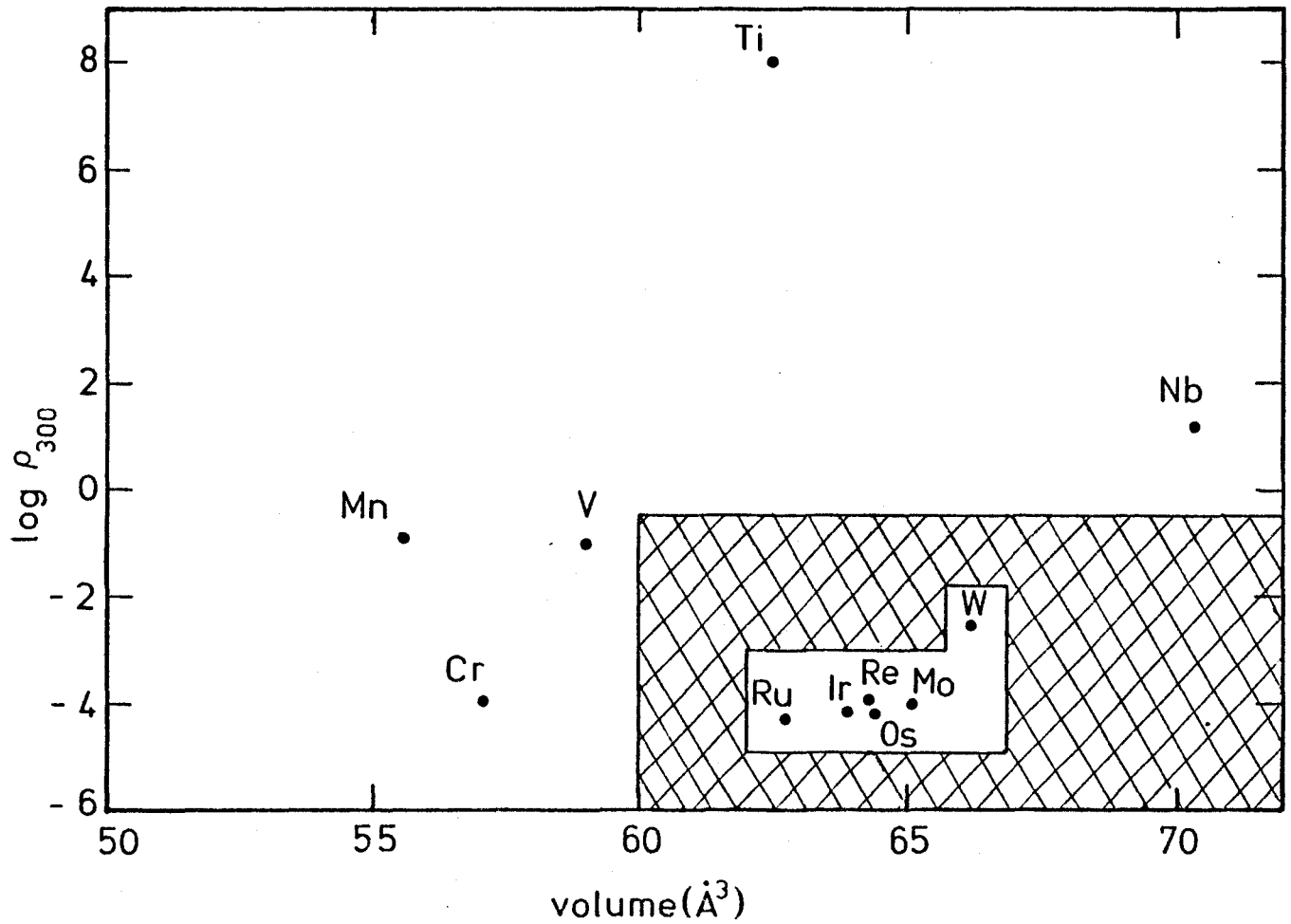

Figure 1.1 Resistivity versus unit cell volume for rutile related transition metal dioxides (from Murphy and Christian 1979). Those in shaded area readily incorporate lithium.

conductivity is not a general requirement for lithium insertion in transition metal dioxides, as anatase TiO_2 (Whittingham and Dines 1977) and γ-MnO_2 (Ikeda et al 1975), which are 10 and 16 percent less dense than their rutile polymorphs and poor electronic conductors, incorporate substantial amounts of lithium.

The group at Bell Labs prepared the lithium intercalates of numerous rutile-related transition metal dioxides by reaction with n-butyl lithium in hexane (Murphy et al 1978). They determined the approximate cell parameters of these compounds by indexing X-ray powder diffraction data to "pseudotetragonal" cell parameters (Table 1.1). These data indicate that lithium intercalation in these compounds is generally accompanied by a substantial expansion in the a direction and a smaller contraction along the c axis, resulting in a volume increase of 10 to 20% for materials incorporating one or more lithium ions per dioxide molecule. It was found that lithium could be removed from the host cell by reaction with water at room temperature (Murphy et al 1978); such mild conditions for recovery of the host cell suggest a similarity in structure between Li_xMO_2 and MO_2. From a magnetic susceptibility study of the Li_xMO_2 (M = Mo, W, Os, Ir and Ru) materials with $x \geq 1$, it was observed that these compounds are metastable, having decomposition temperatures ranging from a low of 340 K for $LiWO_2$ to a high of 475 K for $LiMoO_2$ (Di Salvo et al 1979/80).

Table 1.1

Crystallographic Parameters for Rutiles

and Lithiated Rutiles (From Murphy et al 1978)

	a(Å)	c(Å)	c/a	V(Å^3)	ΔV/V	dec T(°C)[a]
TiO_2	4.594	2.958	0.644	62.4		
VO_2[b]	4.552	2.846	0.625	58.97		
CrO_2	4.422	2.916	0.660	57.02		
$Li_{0.8}CrO_2$	4.84	2.88	0.595	67.5	0.184	
MnO_2	4.398	2.874	0.653	55.58		
NbO_2[b]	4.567	2.994	0.618	70.297		
MoO_2[b]	4.82	2.80	0.581	65.05		
$Li_{1.0}MoO_2$[b]	5.13	2.78	0.542	73.16	0.125	210
WO_2[b]	4.88	2.78	0.570	66.20		
$Li_{1.0}WO_2$[b]	5.16	2.75	0.533	73.22	0.106	80
RuO_2	4.491	3.106	0.692	62.64		
$Li_{1.3}RuO_2$[b]	5.043	2.784	0.552	70.80	0.130	210
OsO_2	4.497	3.182	0.708	64.36		
$Li_{1.5}OsO_2$[b]	5.162	2.795	0.541	74.45	0.157	
IrO_2	4.499	3.155	0.701	63.85		
$Li_{1.5}IrO_2$[b]	4.873	3.190	0.655	75.75	0.186	>80
$Mo_{.5}V_{.5}O_2$	4.64	2.86	0.616	61.66		
$Li_{1.0}Mo_{.5}V_{.5}O_2$	5.06	2.79	0.551	71.43	0.158	130

[a] Values determined by irreversible magnetic susceptibility changes.

[b] Pseudotetragonal parameters.

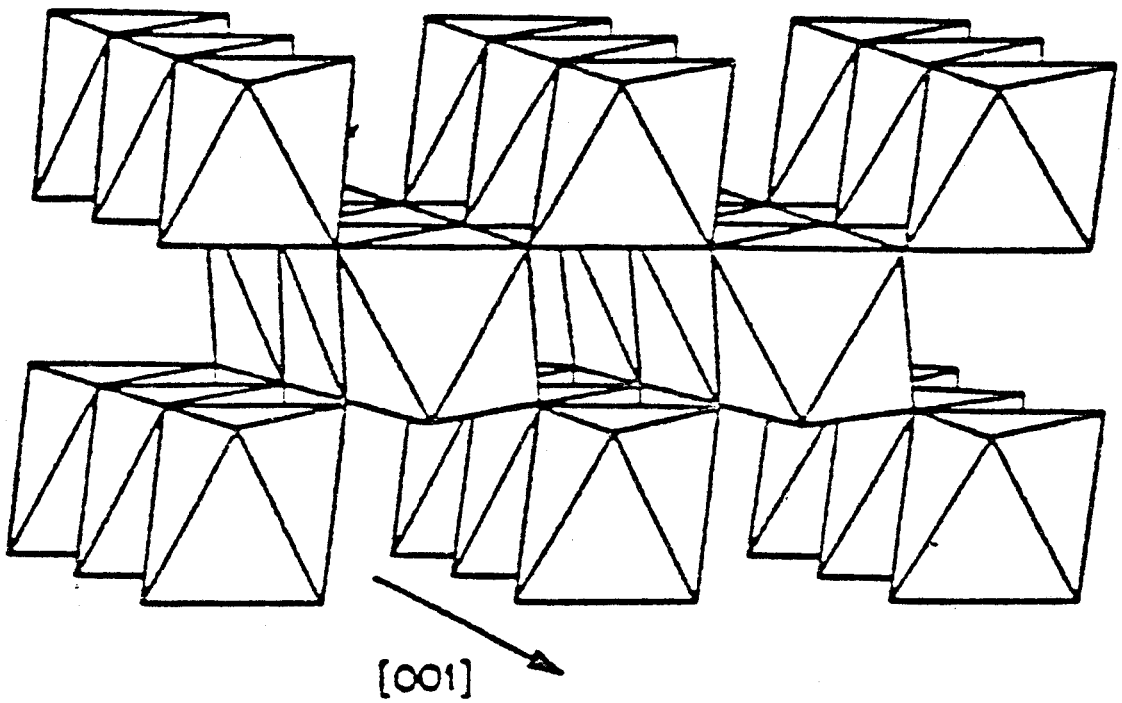

Figure 1.2 Projection of rutile structure showing channels available for lithium insertion (from Murphy et al 1978).

The ideal rutile structure can be viewed as a distorted hexagonal close packing of oxygen atoms in which metal atoms, octahedrally coordinated by oxygen, form infinite chains along the c-direction; these chains of octahedra share corners leaving an equal number of identical vacant channels between them (Fig. 1.2). Murphy et al pointed out that these vacant channels, with two tetrahedral and one octahedral site per metal ion, contain the most probable sites for the intercalated lithium ions (Murphy et al 1978). The octahedral sites (Fig. 1.3) which correspond to the 4(c) sites of the rutile space group, $P4_2/mnm$, are at either $0\frac{1}{2}0$ and $\frac{1}{2}0\frac{1}{2}$ or $0\frac{1}{2}\frac{1}{2}$ and $\frac{1}{2}00$ (both sets of sites can not be filled without overlapping the coordination octahedra) while the tetrahedral sites (Fig. 1.4), which correspond to the 4(d) sites of the rutile space group, are at $0\frac{1}{2}\frac{1}{4}$, $0\frac{1}{2}\frac{3}{4}$, $\frac{1}{2}0\frac{1}{4}$ and $\frac{1}{2}0\frac{3}{4}$. The six-coordinated sites (Fig. 1.5) have two bond lengths much shorter than the other four (about 1.63 Å and 2.25 Å respectively in RuO_2) while the four-coordinated sites (Fig. 1.6) have all bond lengths equal (about 1.80 Å in RuO_2). Since the crystal radius of Li^+ is 0.90 Å for six-coordination and 0.73 Å for four-coordination while that of O^{2-} is 1.26 Å (Shannon 1976), some distortion of the oxygen octahedra on intercalation must be expected. If the distortion is towards more ideal hexagonal close packing of the oxygen lattice, then one set of octahedral interstices will be considerably larger than the tetrahedral ones (Adams 1974), and therefore, might be the preferred sites for lithium

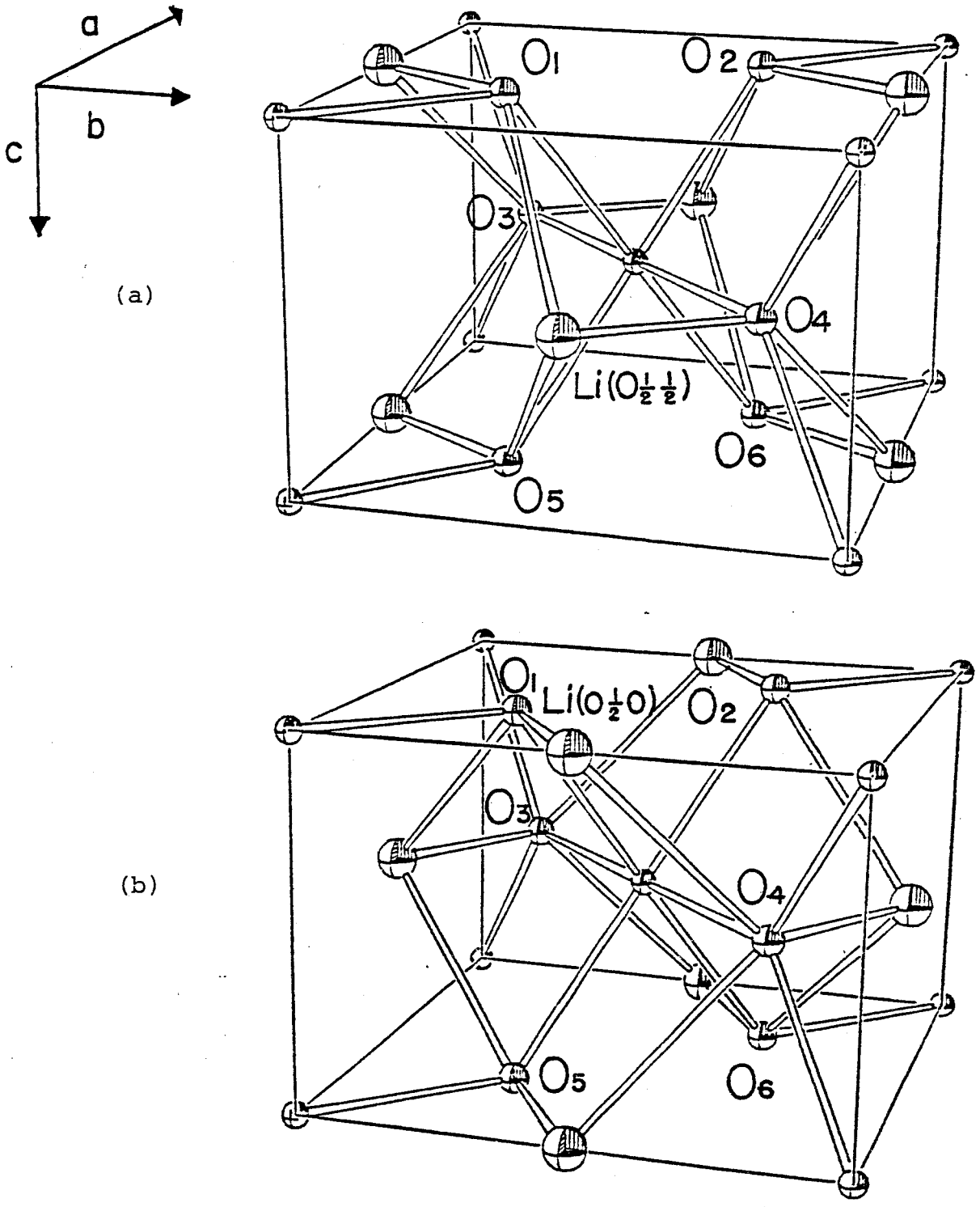

Figure 1.3 Lithium in octahedral sites of rutile (RuO_2) cell at (a) 0½½ and ½00, and (b) 0½0 and ½0½.

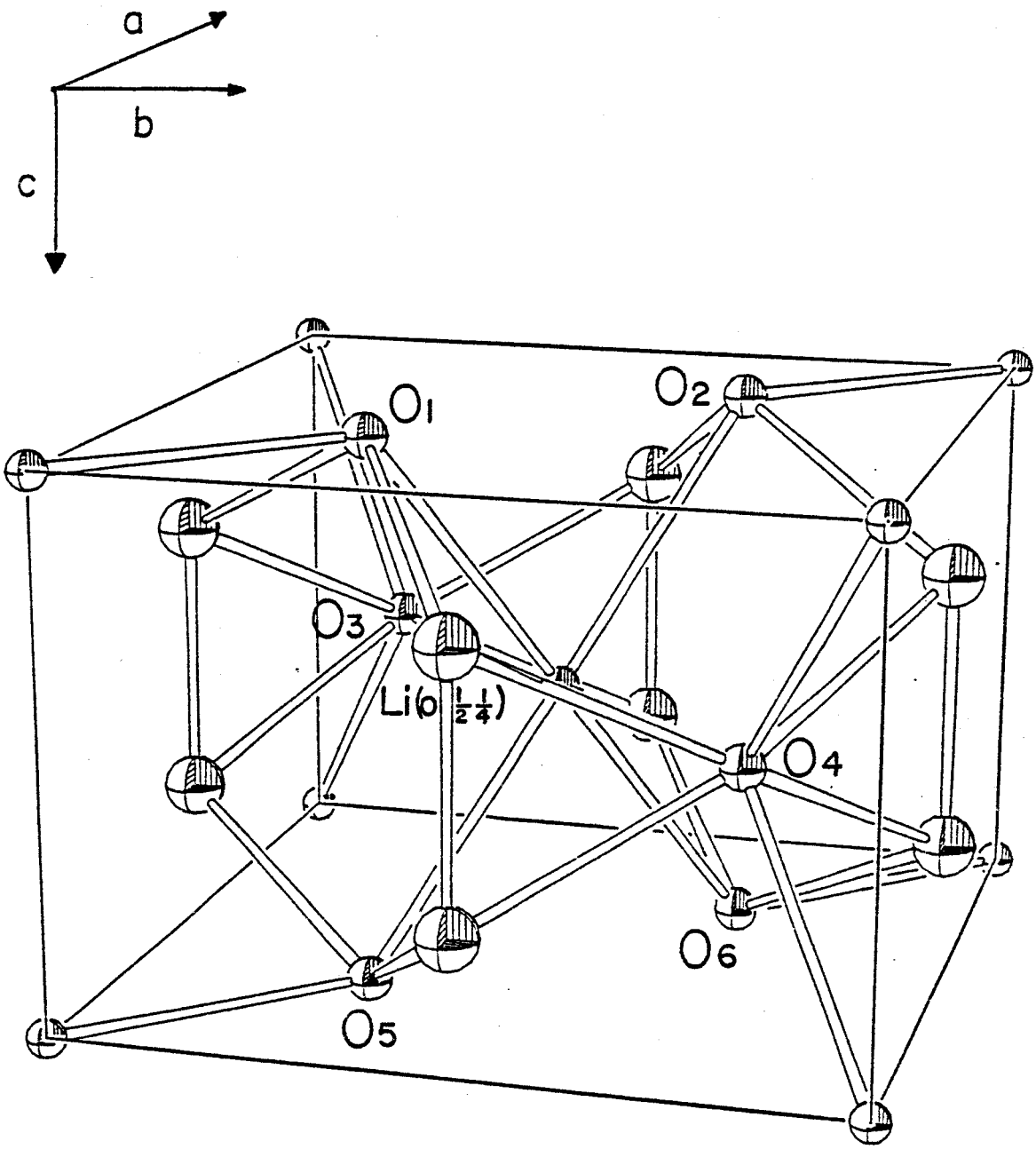

Figure 1.4 Lithium in tetrahedral sites of rutile (RuO_2) cell at $0\frac{1}{2}\frac{1}{4}$, $0\frac{1}{2}\frac{3}{4}$, $\frac{1}{2}0\frac{1}{4}$ and $\frac{1}{2}0\frac{3}{4}$.

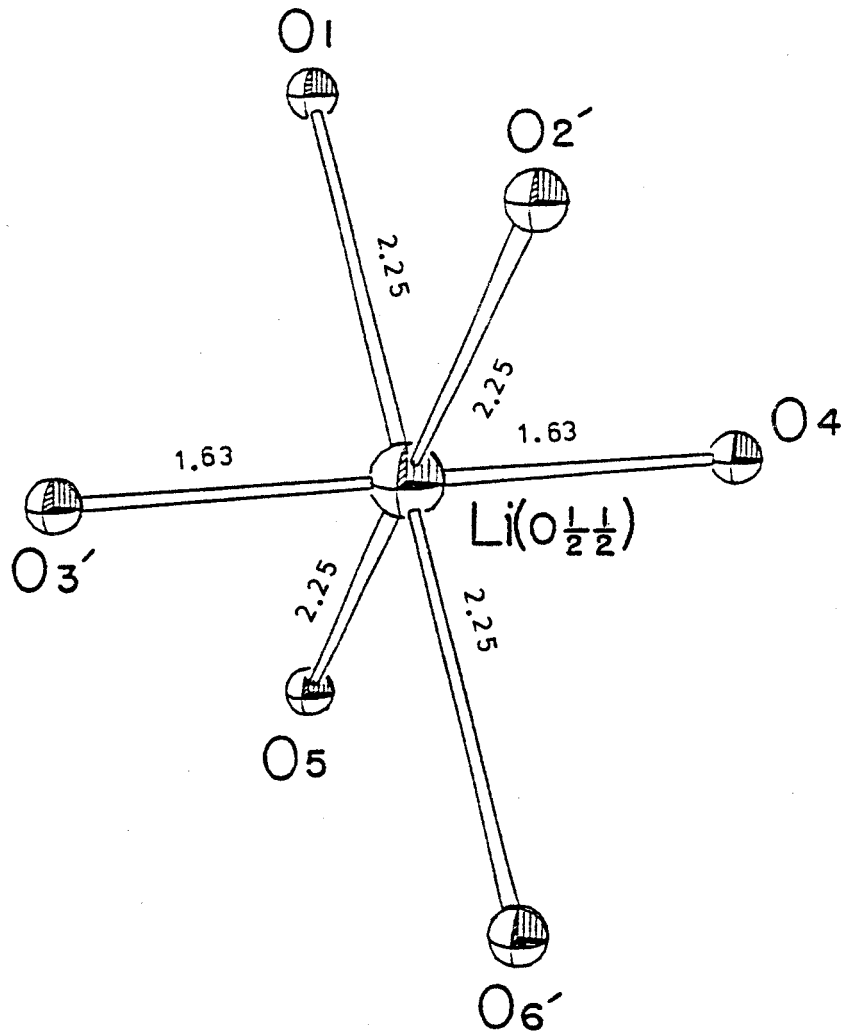

Figure 1.5 Geometry of octahedral site in rutile (RuO_2) cell.

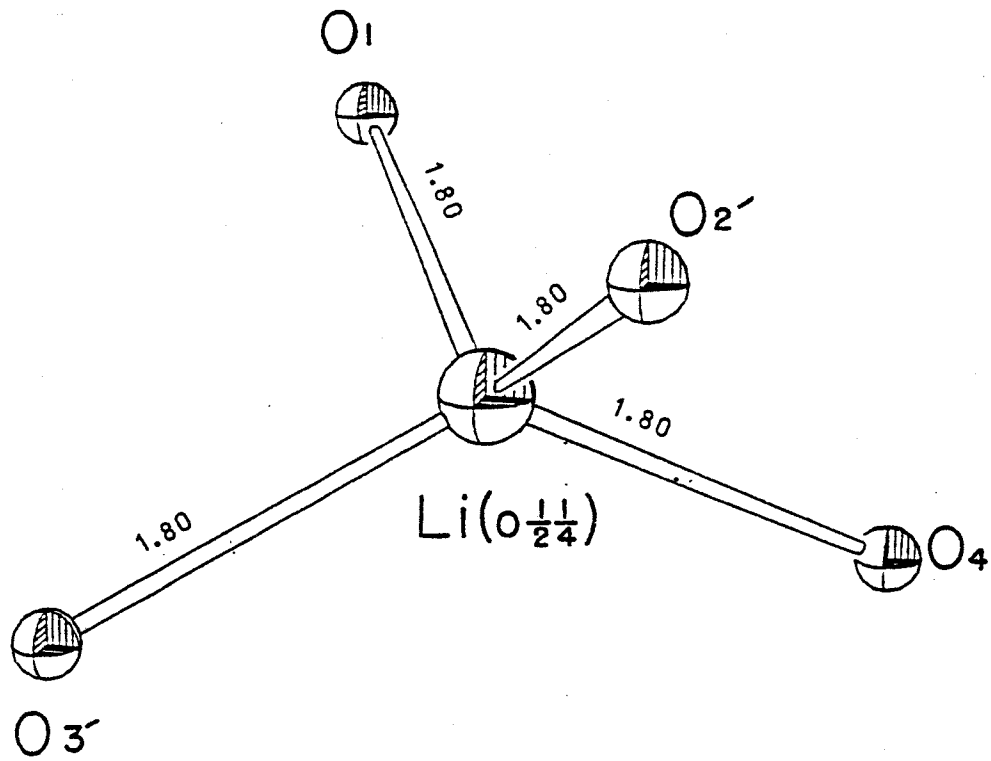

Figure 1.6 Geometry of tetrahedral site in rutile (RuO_2) cell.

insertion. It is perhaps valuable to note that, in the tetragonal rutile space group, the two pairs of octahedral interstices belong to the same crystallographic site, 4(c), and thus, the ordered occupancy of only one pair of octahedral holes would require that the intercalation product belong to a crystal class of lower symmetry, such as orthorhombic or monoclinic.

Alternatively, from crystal packing considerations, it has been suggested (Baur 1981) that it may be energetically more favourable for some or all of the cations to be tetrahedrally coordinated. Baur pointed out that the anions in a theoretical rutile type packing with ideal octahedral coordination are actually close packed. He named this packing tetragonal close packing because the overall symmetry of the arrangement is tetragonal. In this packing scheme each sphere is surrounded by eleven nearest neighbours to form the densest equivalent packing next to the traditional closest packings (Fig. 1.7). The rutile structure is generally viewed as a distorted hexagonal close packed oxygen lattice with metal atoms occupying alternate octahedral interstices in chains along [001]. In hexagonal close packing, filling of more tetrahedral holes than there are close packed atoms results in energetically unfavourable sharing of faces between coordination tetrahedra. An interesting property of tetragonal close packing is that 25% more tetrahedral interstices can be filled without resulting in face sharing (Baur 1981).

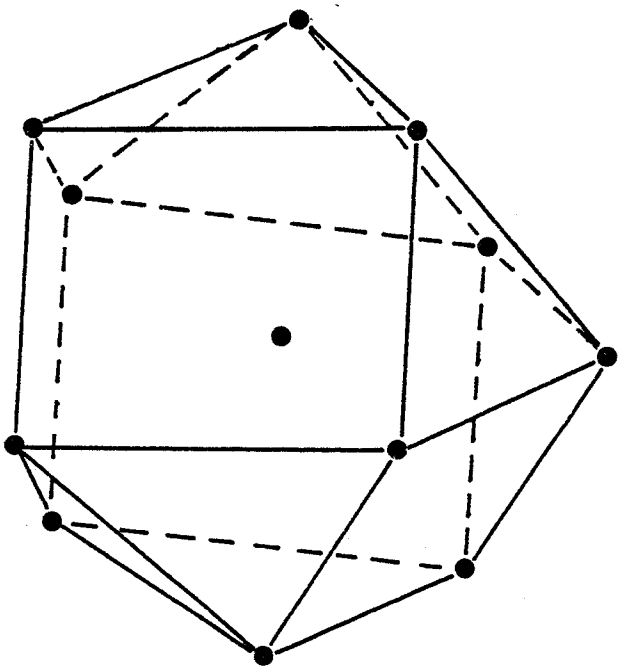

Figure 1.7 Tetragonal close packing (from Baur 1981).

Li_4GeO_4, $Li_{1.5}IrO_2$ and $Li_{1.5}OsO_2$ are all examples of compounds with 1.25 cations to 1 close packed anion. In Li_4GeO_4 all the cations are 4-coordinated (Vollenkle and Wittmann 1969), though the oxygen framework is essentially the same as in the rutile, GeO_2, where the cations are 6-coordinated. The Ge and Li(1) atoms in Li_4GeO_4 occupy the same channels as do the Ge atoms in GeO_2, while the Li(2) atoms occupy the channels parallel to [001], which were vacant in GeO_2.

It has been proposed that the lithium ions occupy the vacant channels of the host rutile parallel to [001] in $Li_{1.3}RuO_2$, $Li_{1.5}OsO_2$ and $Li_{1.5}IrO_2$ (Murphy et al 1978). These lithiated dioxides have c/a ratios smaller than the parent rutiles. In the cases of $Li_{1.3}RuO_2$ and $Li_{1.5}OsO_2$ the c/a ratios, 0.552 and 0.541 respectively (Table 1.1), are close to the ideal value for tetragonal close packing, 0.586 (Baur 1981). Thus, Baur suggested that some or all of the cations in these compounds may be tetrahedrally coordinated.

Intercalation materials can not generally be prepared as single crystals, presumably because the expansion and change of symmetry of the host lattice fractures the crystal. Thus, their structures must be determined by powder diffraction techniques. X-ray data can give information about the unit cell and the positions of the heavy atoms, but is not capable of locating lithium in the presence of heavy transition metals because of the enormous difference in the scattering amplitudes of the two atoms. For neutron scattering,

however, the relative difference between the scattering amplitude of lithium and the other atoms present in these compounds is much smaller and thus, neutron powder diffraction will be used to determine the structure of these intercalation compounds.

Very few structures of lithium insertion compounds of metal oxides have been determined; the structures of Li_xReO_3 (Cava et al 1982) and $LiMoO_2$ (Cox et al 1982) were reported while this work was in progress. Additional structures are needed to further the understanding of this class of compounds and of the intercalation process.

Given the two models described earlier, the aim of this thesis is to elucidate the structural properties of Li_xMO_2 (M = Ru, Os and Ir) by X-ray and neutron powder diffraction, with the object of clarifying the importance of crystal packing factors in this class of compounds.

The theory of neutron scattering will be discussed in a separate chapter on structure determination, as will be the treatment of diffraction data and the results of the structure refinements. The preparation and characterization of intercalates, and descriptions of the diffraction instruments will be given in the following chapter.

CHAPTER 2

DESCRIPTION OF EXPERIMENT

2.1 Preparation of Intercalation Compounds

2.1.1 Li_xRuO_2

Polycrystalline RuO_2 was prepared by heating amorphous RuO_2 (Atomergic Chemical Co.) in air in a platinum crucible to 900°C for a minimum of 15 hours. The black product was then finely ground and dried for 18 hours at 150°C. The lithium intercalate, Li_xRuO_2, was formed on exposure of the host dioxide, RuO_2, to a 0.2 M solution of n-butyl lithium (Aldrich Chem. Co.) in hexane for one to two weeks at ambient temperature. Since both the reagent, n-butyl lithium, and the intercalation product decompose on contact with air or moisture, the reaction was carried out in closed flasks in a dry box under an argon atmosphere. The hexane (reagent grade from Caledon Labs Ltd.) was dried by refluxing it over CaH_2 for a minimum of 12 hours, and was later stored over 4 Å molecular sieves (Fisher Scientific Co.). After one to two weeks of reaction, the hexane solution was decanted off the solid black intercalation product with the aid of a hypodermic syringe and the material was then rinsed twice with about 25 ml of hexane and dried under vacuum for about two hours. Compositions with smaller

amounts of lithium (x = 0.15 and 0.26, for example) were prepared by decreasing the quantity of n-butyl lithium used. In these preparations about half of the lithium present in the solution was incorporated in the product. Attempts to prepare samples having large quantities of lithium, that is with x > 1, by increasing the concentration of n-butyl lithium in solution did not give consistent results. Apparently, other factors such as duration of reaction also play a role in determining the amount of lithium inserted into the host cell.

2.1.2 $\underline{Li_xOsO_2}$

In an attempt to assure the purity of the product, crystals of OsO_2 were prepared by a gas transport technique (Rogers et al 1971). This preparation involves the oxidation of Os metal and subsequent transport of OsO_2 by reaction with O_2 produced "in situ" from the thermal decomposition of $NaClO_3$:

$$3Os + 2NaClO_3 \rightarrow 3OsO_2 + 2NaCl$$

$$OsO_2(s) + O_2(g) \rightleftarrows OsO_4(g).$$

Both the initial preparation of polycrystalline OsO_2, and the subsequent crystal growth were carried out in a sealed quartz tube of length 21 cm and internal diameter 1.8 cm. The Os powder (obtained from Alfa Products) was dried under vacuum for three hours at 100°C. The quartz tube was throughly

washed with distilled water and degassed by heating to redness under vacuum. To facilitate sealing off, the quartz tube was constricted at the appropriate length before loading. The osmium metal and $NaClO_3$ were transferred to the quartz tube through a long-stemmed funnel, and the tube was then sealed under vacuum. Following the procedure of Rogers et al, enough $NaClO_3$ was added to the reaction mixture to provide a 0.2 atm excess of oxygen over that required to convert all the osmium metal to the dioxide. During the sealing procedure, heating of the $Os/NaClO_3$ mixture was prevented by wrapping the bottom of the tube in a wet cloth, and loss of fine powder to the vacuum system was obstructed by inserting a glass wool plug between the vacuum system and the constriction in the quartz tube.

The sealed tube was then heated slowly (50°/hr) in a horizontal tube furnace to 300°C and left overnight. The temperature was then raised to 650°C for three hours to permit the decomposition of $NaClO_3$ and the formation of OsO_2. The 0.2 atm excess of oxygen formed from the decomposition of $NaClO_3$ serves as the transport gas for the subsequent crystal growth, and the NaCl produced as a by-product of the reaction has no detrimental effect. For the transport reaction the temperature was raised to 960°C. The tube had been positioned in the furnace such that while the charge was maintained at 960°C, the growth region of the tube was at approximately 900°C.

After seven days of growth, the tube was cooled to room temperature and opened. About 85% of the charge had been transported, forming shiny golden crystals of OsO_2. The remainder of the material was present as black Os metal and yellow OsO_4 crystals. Li_xOsO_2 was prepared from the OsO_2 crystals, after they were finely ground and dried at 100°C for several hours, by treating them with n-butyl lithium as described earlier.

2.1.3 Li_xIrO_2

Crystals of IrO_2 were prepared by a gas transport reaction involving the oxidization of Ir sponge in a stream of dry O_2 at 1000°C and subsequent transport of IrO_2 via the higher oxide, IrO_3 (Rogers et al 1971):

$$Ir(s) + O_2 \rightarrow IrO_2(s)$$

$$IrO_2(s) + \tfrac{1}{2}O_2(g) \rightleftarrows IrO_3(g).$$

The iridium sponge (7 g from Johnson-Matthey Ltd.) was placed into two alumina boats which were then loaded into a silica tube of internal diameter, 13 mm, and length 63 cm. The tube was inserted into a horizontal tube furnace which was fitted with lubricated ground glass joints to a gas inlet tube at one end and a water bubbler at the other. The oxygen flow was set at 17 cc/min and the furnace was heated to 1000°C for 24 hours to oxidize the iridium metal. The charge was then heated to 1190°C resulting in the formation of $IrO_3(g)$.

Most of the transported material was deposited near the ends of the tube where the temperature was approximately 1000°C.

After two weeks, only about 8% of the charge had been transported. The products were purplish-black polyhedral chunks and flat plates of IrO_2, which adhered strongly to the quartz tube. The material left in the alumina boats was a very hard greyish-black mass of partially oxidized Ir metal, even though the boats had been initially loaded with finely ground powder. This suggested that the Ir metal sintered together before it could all be oxidized, making oxygen diffusion difficult. Increasing the metal surface area and the oxygen flow rate resulted in a small increase in the yield, producing fine black needles of IrO_2.

More complete reaction was obtained by exposing the Ir/IrO_2 mixture to a higher pressure of O_2. This was accomplished by sealing the Ir/IrO_2 mixture in a quartz tube with a chemical source of oxygen, $NaClO_3$, and heating it to 1190°C for two days in an rf-generating furnace. The reaction proceeds by a mechanism similar to that for the preparation of OsO_2 described earlier:

$$3Ir + 2NaClO_3 \rightarrow 3IrO_2 + 2NaCl$$

$$IrO_2(s) + \tfrac{1}{2}O_2(g) \rightleftarrows IrO_3(g).$$

Pressures of up to 4 atm (at 1190°C) were supported by the quartz tube by pressurizing the furnace chamber to about 2 atm with argon.

Once loaded, the quartz tube was placed vertically in the rf-furnace with the bottom of the tube (where the charge was) enclosed in a graphite susceptor. Throughout the growth procedure, the top of the tube was much colder than the charge, perhaps even close to room temperature. The Ir/IrO_2 mixture reacted with the O_2 generated from the thermal decomposition of $NaClO_3$ to form $IrO_3(g)$, which was then transported up the tube by convection and deposited in the cooler region as fine needles of IrO_2.

Li_xIrO_2 was prepared from IrO_2, which had been dried overnight at 110°C, and n-butyl lithium as previously described.

2.2 Characterization of Intercalation Compounds

2.2.1 Chemical Analysis

The lithium content of the intercalation products was determined by atomic absorption and/or by direct titration. Both methods required submerging the compound in water to draw out the intercalated lithium as LiOH. By the direct titration method, the LiOH in solution was reacted with an excess of HCl and the quantity in excess was determined by back titration with NaOH. The analyses by atomic absorption used Li_2CO_3 as a standard.

2.2.2 X-ray Powder Diffraction

The lattice parameters of the intercalated materials were determined from X-ray powder diffraction data collected on a Philips diffractometer with graphite monochromatized

CuK_α radiation using KCl as an internal standard. Data were collected over the range of about $20° \leq 2\theta \leq 80°$ with a scan rate of ½°/min. Generally about 9 or 10 well resolved peaks were obtained, from which the lattice parameters were determined with the aid of a least squares refinement program.

The intercalation products, Li_xMO_2 (M = Ru, Os and Ir), decompose very rapidly on exposure to air or moisture and consequently, must be protected from air while the X-ray diffraction pattern is obtained. To accomplish this, the samples were prepared in an argon dry box by pressing the finely ground powder into a vertical groove in a glass slide, and covering the slide with a piece of transparent tape, fitted with a plastic ("Handiwrap") window, which was large enough to expose the vertical groove. This served to prevent sample decomposition, while getting enough material into the x-ray beam to produce a reasonably intense powder diffraction pattern. It was found that the plastic window produced a broad peak around 21.5 in 2θ, perhaps due to short range order, and that it increased the background at low angles ($2\theta < 28°$). This, however, did not seriously affect the diffraction peaks of the materials studied.

2.3 Neutron Diffraction

All the neutron diffraction data for this work were collected on the triple axis spectrometer (in double axis mode) at McMaster University Research Reactor. This instrument has been described in detail previously (Rowe 1976).

The data were collected at a monochromatic neutron wavelength of 1.40 Å obtained from the (200) reflection of a single crystal of copper. Instrumental parameters such as the zero angle, precise wavelength and resolution were determined from the diffraction pattern of finely divided polycrystalline copper. The spectrometer is equipped with a position sensitive detector, which consists of two 2.54 cm diameter, 61 cm long ^{3}He detectors mounted horizontally one above the other. In its present configuration, this instrument is capable of detecting neutrons scattered over 35° in 2θ. For the neutron diffraction experiment, the samples were loaded in an Ar atmosphere into 4 or 8 mm diameter, thin walled, cylindrical vanadium cans, which were sealed with a flat teflon gasket to protect the materials from exposure to air.

CHAPTER 3

DETERMINATION OF STRUCTURES

3.1 Introduction

In this section, the theory of X-ray and neutron diffraction as it pertains to the determination of crystal structures will be discussed. This discussion will closely follow related chapters in Kittel (1976) and in Ashcroft and Mermin (1976). A description, taken largely from Woolfson (1970) and Cullity (1956), of the important role of symmetry in determining the unit cell shape and dimensions, and the atomic positions is presented. The theory and procedure for refining structures from X-ray and neutron powder diffraction intensities will be developed in some detail.

3.1.1 Theory of Diffraction

Just as visible light is diffracted by a ruled grating, any waves will be diffracted by an evenly spaced array of scattering objects provided that the wavelength is of the same order of magnitude as the separation between the scatterers. Diffraction is an interference effect caused by the mutual reinforcement of a large number of scattered waves.

In a crystal, interatomic spacings are generally on the order of 1 Å. Thus, any radiation which is scattered by

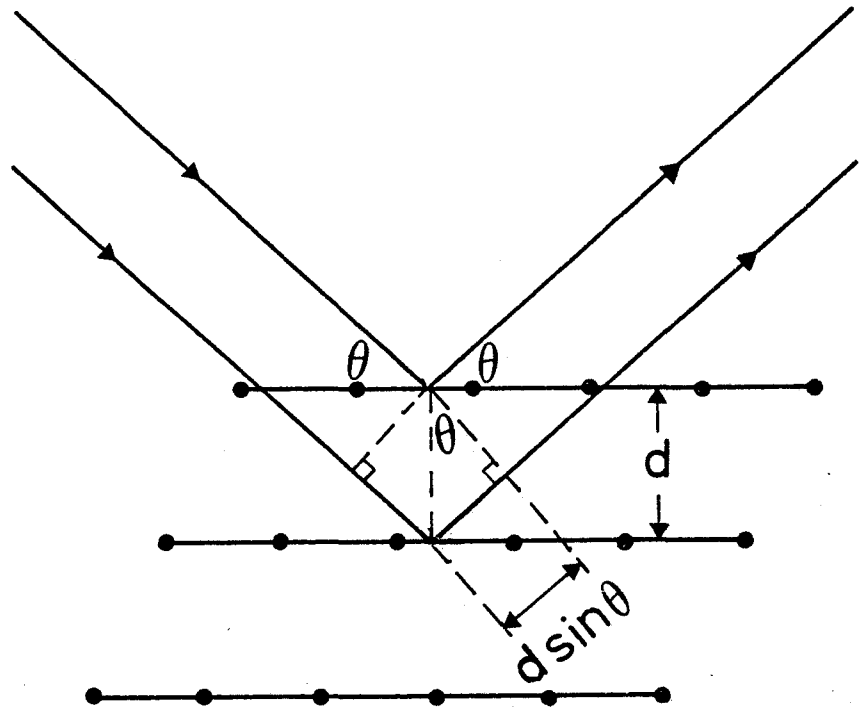

Figure 3.1 Bragg reflection from a family of lattice planes. The path difference between rays scattered from successive planes is $2d\sin\theta$.

atoms and has a wavelength of about 1 Å will be diffracted by crystals. Both X-rays and neutrons can fulfill these requirements.

The condition for constructive interference of radiation scattered from crystalline materials was determined by both Bragg and Laue. Though their approaches differ, their results are equivalent. Bragg pictured a crystal as being formed from uniformly spaced parallel planes of ions. He accounted for diffraction by envisioning an incident ray as being reflected by the plane of ions such that the angle of reflection is equal to the angle of incidence, θ. Under this condition rays reflected from successive planes interfere constructively whenever their path difference is an integral multiple of the wavelength of the radiation. From Figure 3.1 it can be seen that the path difference is $2d\sin\theta$, giving the famous Bragg condition,

$$m\lambda = 2d\sin\theta$$

for integral m.

The approach of Laue can be outlined by considering an incident beam travelling in direction $\hat{n}$, which is scattered by two atoms separated by a vector $\vec{d}$, without any exchange of energy. Again the scattered rays will interfere constructively when the path difference between the rays is an integral number of wavelengths. Thus, from Figure 3.2, the condition for constructive interference is

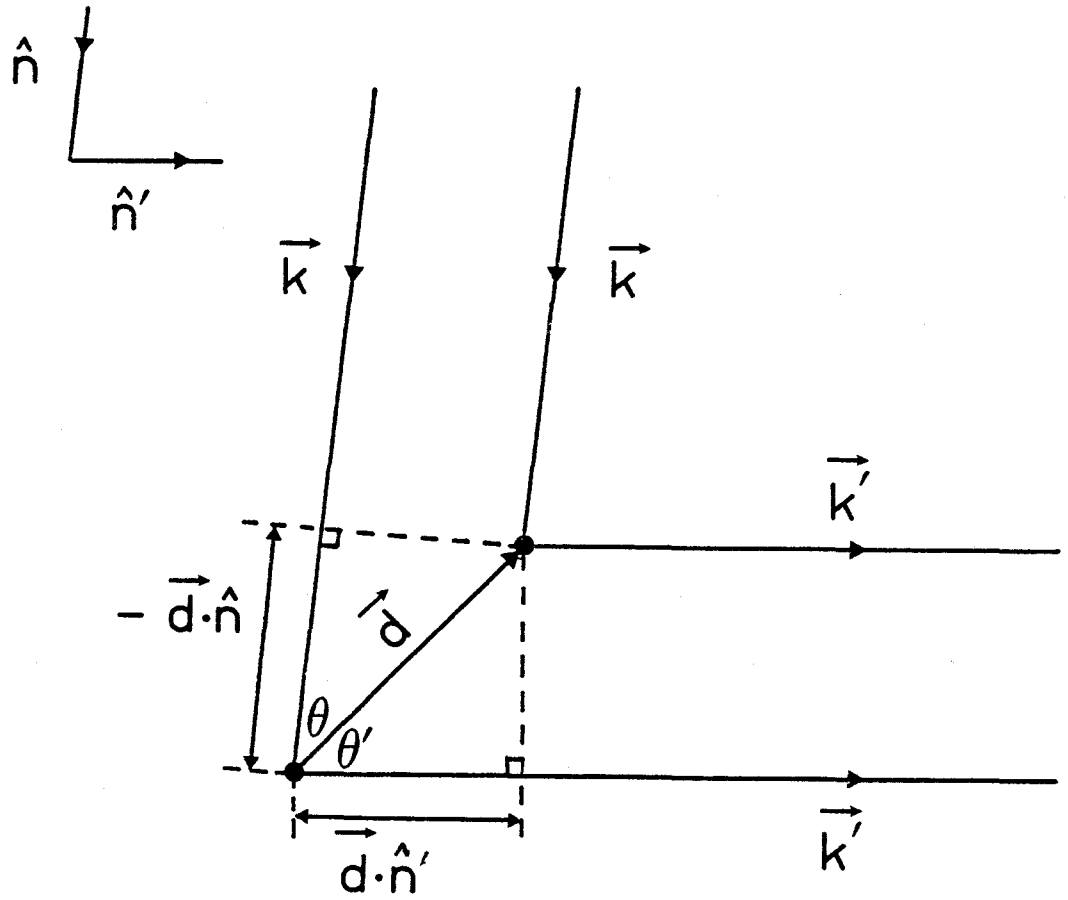

Figure 3.2 Laue condition for constructive interference. The path difference between rays scattered from two atoms separated by a vector $\vec{d}$ is $\vec{d}\cdot(\hat{n}' - \hat{n})$.

$$\vec{d}\cdot(\hat{n}' - \hat{n}) = m\lambda$$

where $\hat{n}'$ is the direction of the scattered beam and m is an integer. In terms of the wavevectors $\vec{k}$ and $\vec{k}'$ of the incident and scattered beams respectively, this can be rewritten as

$$\vec{d}\cdot(\vec{k}' - \vec{k}) = 2\pi m.$$

If as in a simple Bravais lattice the atoms are separated by lattice vectors $\vec{R}$ then the requirement for constructive interference becomes

$$\vec{R}\cdot(\vec{k}' - \vec{k}) = 2\pi m$$

or

$$e^{i\Delta\vec{k}\cdot\vec{R}} = 1$$

for all $\vec{R}$, where

$$\Delta\vec{k} = \vec{k}' - \vec{k}.$$

This restriction is equivalent to saying that the momentum transfer, $\Delta\vec{k}$, must be the wavevector of a plane wave which has the periodicity of the Bravais lattice:

$$e^{i\Delta\vec{k}\cdot(\vec{R}+\vec{r})} = e^{i\Delta\vec{k}\cdot\vec{r}}$$

for any $\vec{r}$. The set of all wavevectors which satisfy this condition is called the reciprocal lattice. The reciprocal lattice is itself a Bravais lattice and can be described by three primitive vectors $\vec{A}$, $\vec{B}$, $\vec{C}$, which are related to the primitive vectors $\vec{a}$, $\vec{b}$, $\vec{c}$ of the direct lattice by the following relationships:

$$\vec{A} = \frac{2\pi \vec{b}\times\vec{c}}{\vec{a}\cdot(\vec{b}\times\vec{c})} , \quad \vec{B} = \frac{2\pi \vec{c}\times\vec{a}}{\vec{a}\cdot(\vec{b}\times\vec{c})} , \text{ and } \vec{C} = \frac{2\pi \vec{a}\times\vec{b}}{\vec{a}\cdot(\vec{b}\times\vec{c})} .$$

Therefore any point in the reciprocal lattice can be described by a reciprocal lattice vector

$$\vec{G} = h\vec{A} + k\vec{B} + l\vec{C}.$$

The reciprocal lattice vectors are commonly used to designate families of planes in the direct lattice. From the definition of a reciprocal lattice vector, it can be shown that every family of lattice planes has a reciprocal lattice vector normal to it (Ashcroft and Mermin 1976). If the lattice planes are separated by a distance d, then the shortest reciprocal lattice vector normal to it will be of length $2\pi/d$. The coordinates of the shortest reciprocal lattice vector normal to the plane with respect to the primitive reciprocal lattice vectors are known as Miller indices. For example, a plane with Miller indices (hkl) is normal to the reciprocal lattice vector

$$\vec{G} = h\vec{A} + k\vec{B} + l\vec{C}.$$

In terms of the direct lattice, the Miller indices are the reciprocals of the fractional intercepts between the plane and the crystallographic axes, a, b, c. Therefore the plane described by the Miller indices (hkl) has intercepts a/h, b/k, c/l.

The Laue condition for constructive interference

requires that

$$\Delta\vec{k} = \vec{k}' - \vec{k} = \vec{G}$$

be a reciprocal lattice vector. Since the scattering is elastic $\vec{k}$ and $\vec{k}'$ must have the same magnitude, and therefore, must make the same angle θ with respect to the plane perpendicular to $\vec{G}$. Thus, from Figure 3.3 it can be seen that

$$G = 2k\sin\theta.$$

If $\vec{G}$ is a reciprocal lattice vector, its length must be an integral multiple of the length of the shortest reciprocal lattice vector parallel to it; therefore,

$$G = m2\pi/d$$

for integral m. Since

$$k = 2\pi/\lambda,$$

equating the two expressions for G results in the Bragg law,

$$m\lambda = 2d\sin\theta.$$

Thus, the Laue condition,

$$\Delta\vec{k} = \vec{G}$$

for constructive interference is equivalent to the condition for Bragg reflection from the family of planes normal to $\vec{G}$.

The integer m is generally called the order of the reflection. Rewriting the Bragg equation as

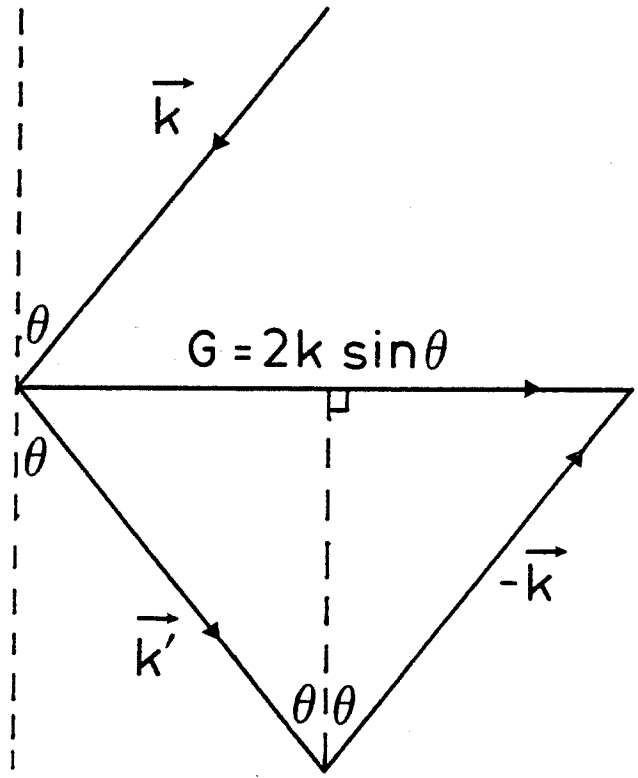

Figure 3.3 Equivalence of Bragg and Laue conditions for diffraction. The Laue condition for diffraction is $\vec{G} = \Delta\vec{k}$. The figure shows that $G = 2k\sin\theta$, but since $G = m2\pi/d$, this is equivalent to the Bragg requirement for diffraction, $m\lambda = 2d\sin\theta$.

$$\lambda = 2\frac{d'}{m}\sin\theta,$$

it can be seen that an m^{th} order reflection from planes separated by a distance d' can be regarded as a first order reflection from real or fictitious planes at a spacing of d'/m. For convenience the Bragg equation is often written as

$$\lambda = 2d\sin\theta,$$

where $d = d'/m$, and an m^{th} order reflection from the planes (hkl) is regarded as a first order reflection from the planes (mh mk ml).

In the powder diffraction method, the material is ground into a fine powder, such that the crystal particles are randomly oriented with respect to the monochromatic incident beam. In this situation, some of the particles will be in the correct orientation to reflect the incident beam from, for example, their (100) planes and others will be correctly oriented to reflect from their (110) planes etc. The net result is that some particles will be in the correct orientation for reflection from any plane and all possible reflections will be observed.

From the Bragg equation, it can be seen that the peak positions, measured in terms of the scattering angle, 2θ, give the interplanar spacings between families of planes with a given set of Miller indices. These spacings can, in turn, be used to determine which crystal system a unit cell belongs to. There are only seven distinct symmetry point groups which

a unit cell can have and these are associated with the seven crystal systems. The seven crystal systems, each represented by a parallelepiped, are described by the relationship between the lengths of the three axes a, b, c and by the values of the three angles between the axes α, β, γ.

The relationship between the interplanar spacings, d, and the lattice parameters (a,b,c, α,β,γ) is well known for each crystal system (Woolfson 1970). However, to fit the lattice parameters one must assign Miller indices to all the observed reflections and this requires that one first make some intuitive guess at which crystal system the material belongs to and the approximate values of the lattice parameters. Fitting programs which search through all the crystal systems for a reasonable fit to the observed d-spacings are available, but they require a large number of reflections to be used successfully. Generally, some "a priori" knowledge of the crystal structure is required for determining the lattice parameters from powder data only.

The best choice of unit cell is not necessarily a primitive one; sometimes a non-primitive cell has a more obvious connection to the point symmetry elements. Bravais has shown that there are only 14 distinct space lattices, 7 primitive and 7 non-primitive, which can completely define the repetition characteristics of a three dimensional pattern without any reference to the repeated motif.

In addition to having a particular point symmetry, a

crystal lattice has elements of translational symmetry. When all the possible symmetry elements of a three dimensional array are considered, there are only 230 distinctive combinations possible; these combinations are called the space groups.

Once the lattice parameters of the unit cell have been determined and the observed Bragg reflections have been assigned Miller indices, a study of the missing reflections can reveal the lattice type (primitive, body-centered, etc.) and the translational symmetry elements of the unit cell. For example, if all the reflections whose Miller indices sum to an odd number are absent (and the apparently absent reflections are not simply too weak to be seen) then the unit cell is body centered. Similarly, consideration of the absence of particular sets of reflections called systematic absences can be helpful in narrowing down the choice of space group.

A crystal structure is defined by its Bravais lattice and by the arrangement of atoms in the unit cell. Information about the arrangement of atoms or basis at any lattice point is obtained from the relative intensities of the Bragg peaks.

If an incoming wave is scattered from two points r_i and r_j (Figure 3.4), the path difference between the scattered rays will be $\Delta\vec{k}\cdot(\vec{r}_i - \vec{r}_j)$ and the phases of the two rays will differ by the factor $e^{i\Delta\vec{k}\cdot(\vec{r}_i-\vec{r}_j)}$. Similarly the rays scattered from $\vec{r}_1 \ldots \vec{r}_n$ will have phases in the ratio $e^{i\Delta\vec{k}\cdot\vec{r}_1}, \ldots, e^{i\Delta\vec{k}\cdot\vec{r}_n}$, and thus, the amplitude of the rays

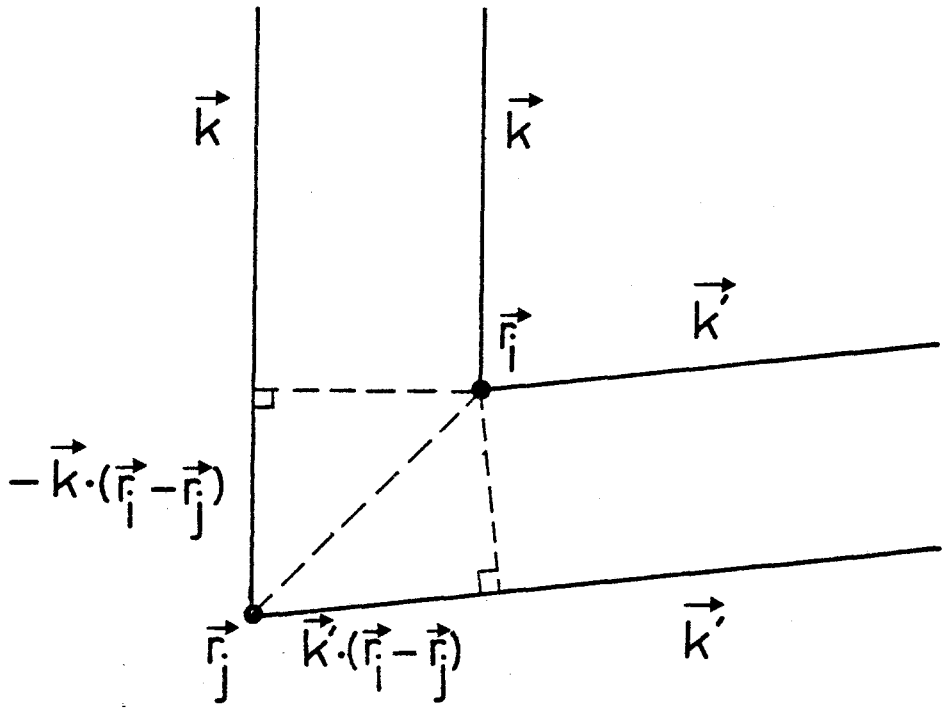

Figure 3.4 Phase difference between rays scattered from two lattice points. The path difference between rays scattered from r_i and r_j is $\Delta\vec{k}\cdot(\vec{r}_i - \vec{r}_j)$ and hence, the phases of the two rays will differ by a factor $e^{i\Delta\vec{k}\cdot(\vec{r}_i - \vec{r}_j)}$.

scattered from the entire primitive cell will contain the factor

$$S_{\Delta\vec{k}} = \sum_{j=1}^{n} e^{i\Delta\vec{k}\cdot\vec{r}_j}.$$

The Laue condition for constructive interference requires that $\Delta\vec{k}$ be a reciprocal lattice vector, $\vec{G}$, and therefore this factor, which is called the structure factor, is associated with a particular Bragg reflection or reciprocal lattice vector and can be expressed as

$$S_{\vec{G}} = \sum_{j=1}^{n} e^{i\vec{G}\cdot\vec{r}_j}.$$

The structure factor indicates the extent to which a particular Bragg reflection is diminished by interference effects between identical ions in the basis. In the case of x-rays, which are electromagnetic radiation, the scattering particles are the electrons, and therefore the total amplitude of the wave scattered from a volume element dV is proportional to the electron concentration in that volume element. Since in general all the atoms in the basis are not identical, the structure factor is modulated by the Fourier transform of electron concentration n_j associated with each atom j. This modulating factor, which is called the atomic scattering factor, is the integral over all space of the electron concentration associated with the j^{th} atom multiplied by a phase factor which depends on the position of the charge relative to the center of the atom. If r = 0 at one corner of the cell and $\vec{r}_j$ is

the vector from the corner of the cell to the center of atom j (Figure 3.5), then the x-ray atomic scattering factor may be written as

$$f_j = \int dV n_j(\vec{r} - \vec{r}_j)\ e^{i\vec{G}\cdot(\vec{r}-\vec{r}_j)}.$$

The x-ray structure factor for any basis is then given by

$$S_{\vec{G}} = \sum_{j=1}^{n} e^{i\vec{G}\cdot\vec{r}_j} \int_{cell} dV\ n_j(\vec{r} - \vec{r}_j) e^{i\vec{G}\cdot(\vec{r}-\vec{r}_j)}$$

or

$$S_{\vec{G}} = \sum_{j=1}^{n} f_j e^{i\vec{G}\cdot\vec{r}_j}.$$

The structure factor can be rewritten in terms of the Miller indices of the reciprocal lattice vector and the fractional coordinates of the atoms in the unit cell:

$$S_{\vec{G}} = \sum_{j=1}^{n} f_j \exp i(h\vec{A} + k\vec{B} + l\vec{C})\cdot(x_j\vec{a} + y_j\vec{b} + z_j\vec{c}).$$

Using the definitions of the primitive reciprocal lattice vectors $\vec{A}$, $\vec{B}$, $\vec{C}$, this expression can be reduced to

$$S_{hkl} = \sum_{j=1}^{n} f_j \exp[2\pi i(hx_j + ky_j + lz_j)].$$

Thus, if the structure factor were known for enough reflections, it would be possible to calculate the positions of all the atoms in the cell. Though the structure factor can not be measured directly, it is proportional to the amplitude of the rays scattered from a unit cell. Since intensity is proportional to the square of the absolute value of the

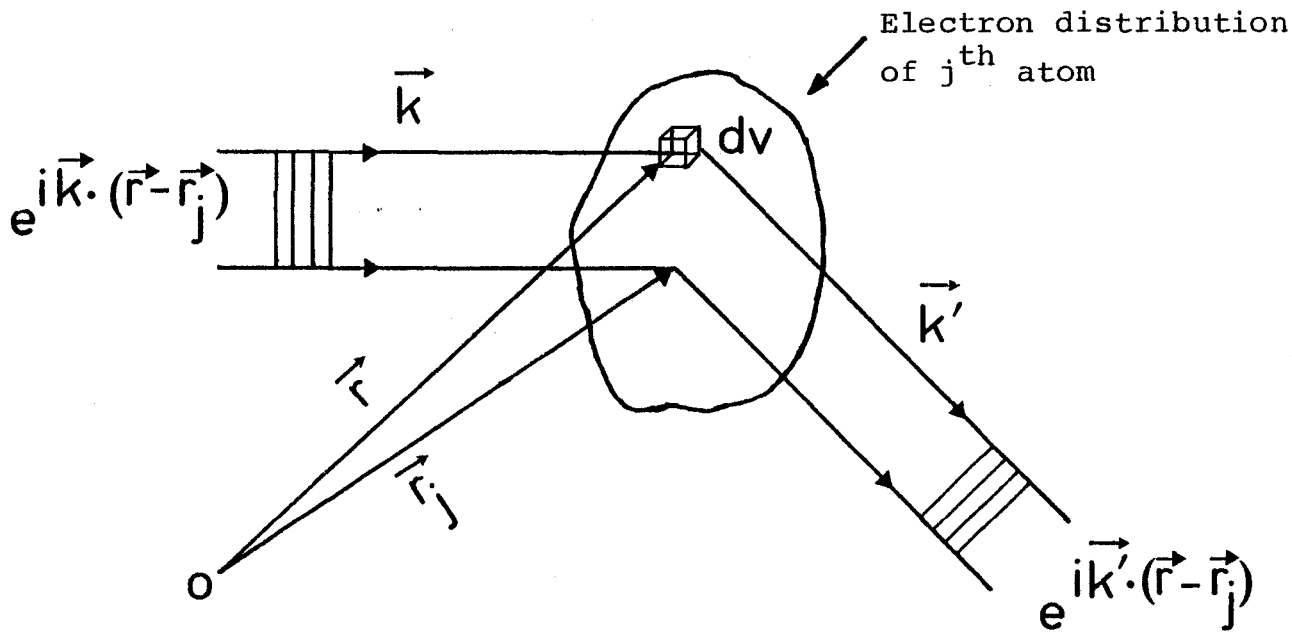

Figure 3.5 Phase difference between rays scattered from electronic charge in a volume element dV and from a charge located at the atomic center, r_j. Since the path difference between the rays is $\Delta k \cdot (\vec{r} - \vec{r}_j)$, their phases differ by a factor $e^{i\Delta k \cdot (\vec{r} - \vec{r}_j)}$.

amplitude, the relative intensities of the Bragg peaks will indirectly provide information about the positions of the atoms in the unit cell.

In the calculation of the structure factor it was tacitly assumed that the atoms in the crystal are tightly bound and not free to move. However, in reality the atoms are subject to thermal vibrations about their equilibrium positions and this motion has the effect of diminishing the amplitude of the coherent scattering by a factor $\exp(-B_j \sin^2\theta/\lambda^2)$, where B_j is a measure of the average displacement of the j^{th} atom and is called the temperature factor. The structure factor thus becomes

$$S_{hkl} = \sum_{j=1}^{n} f_j \exp[2\pi i(hx_j + ky_j + lz_j)]\exp(-B_j \sin^2\theta/\lambda^2).$$

This correction appears as its square, $\exp(-2B_j \sin^2\theta/\lambda^2)$, in the intensity and is then called the Debye-Waller factor.

The X-ray atomic scattering factor is the Fourier transform of the electronic charge distribution of an atom and is dependent on the reciprocal lattice vector. It represents the ratio of the amplitude of the coherent scattered radiation from an atom to that from a single electron situated at the center of the atom.

Coherent elastic scattering of neutrons from non-magnetic atoms also produces Bragg peaks, but in the case of non-magnetic neutron scattering it is the nuclei rather than the electrons which are the predominant scatterers. The

interaction potential between the nucleus and the neutron is of very short range, falling to zero outside a distance on the order of nuclear dimensions ($\sim 10^{-12}$ cm). For diffraction the neutrons must have a wavelength on the order of interatomic distances ($\sim 10^{-8}$ cm). Consequently, the nucleus acts as a point scatterer to neutrons and therefore, the ratio of the amplitude of the coherent scattered radiation from an atom to that of a unit scatterer located at the atomic center is a constant and has no dependence on the reciprocal lattice vector. The neutron structure factor for any basis is then given by

$$S_{hkl} = \sum_{j=1}^{n} b_j \exp[2\pi i(hx_j + ky_j + lz_j)]\exp(-B_j \sin^2\theta/\lambda^2),$$

where b_j is a constant dependent only on the average nuclear structure of the j^{th} atom and is called the neutron scattering length. The scattering length is specific to a given nuclide, and for elements which contain more than one isotope the effective scattering length, $\bar{b}$, is the average value of b weighting eachisotope, r, by its relative abundance, w_r:

$$\bar{b} = \sum_r w_r b_r.$$

The neutron scattering length differs from the X-ray scattering factor in another respect. The X-ray scattering factor is the Fourier transform of the electron charge distribution of a given atom. Therefore, considering only atoms in their zeroth oxidation state, the X-ray scattering factor increases with increasing atomic number through the

concomital addition of an electron. This results in a dramatic difference in the scattering amplitudes of light and heavy atoms. For example, the X-ray scattering amplitude of a lead atom is about 20 times that of a carbon atom (Bacon 1962). The neutron scattering length, however, varies haphazardly through the periodic table such that atoms with quite different atomic numbers can have very similar scattering lengths.

3.1.2 Structure Refinement

At the point where the structure refinement procedure can commence, the chemical composition of the material, and the shape and dimensions of the unit cell (from the fitting of d-spacings) are known, and the choices of space groups have been narrowed down by identifying the systematic absences. In this work, the structure refinement was carried out with the aid of a program called MARYSE (L'Helgoualch et al 1977) which performs a least squares fit to integrated intensities. The least squares refinement attempts to minimize a weighted R-factor, R_w. The weighted R-factor represents the normalized weighted sum of the differences between the observed X-ray or neutron powder diffraction intensities and the intensities calculated from a model structure for the atomic positions. R_w is expressed as

$$R_w = \frac{\sum_i w_i \left[\sum_k I_k(\text{obs}) - \sum_k I_k(\text{calc})\right]}{\sum_i w_i \sum_k I_k(\text{obs})} \times 100$$

where w_i is the weighting factor and the sums are taken over the individual intensities, i, and the overlapping reflections, k. The parameters, with respect to which R_w is minimized, include a scale factor and the fractional coordinates and temperature factors of the individual atoms. To choose a suitable space group and probable atomic sites, a rough model of the structure, usually based on compounds of similar composition or some knowledge of the history of the compound is required.

At the time this work was started there had been no other structures of lithium intercalates of transition metal dioxides reported, though the structure of $LiMoO_2$ appeared in the literature (Cox et al 1982) when this work was almost completed. However, since the compounds being studied, are formed from the parent transition metal dioxide under very mild conditions using a solution of n-butyl lithium in hexane at room temperature, and the host rutile can be recovered under equally mild conditions from Li_xMO_2 by reaction with water at room temperature, it seems reasonable to assume that the structure of the lithium intercalate, Li_xMO_2, must be closely related to that of the host, MO_2.

3.2. TREATMENT OF DATA

3.2.1 X-ray Powder Data

Although lithium is a weak scatterer of X-rays, and therefore, very difficult to locate in the presence of heavy atoms, it should be possible to determine the positions of

the transition metal and oxygen atoms. Data for the structure refinement were collected over the approximate range $20° \leq 2\theta \leq 100°$ in the same manner as was described previously for the determination of the unit cell constants, except that the scan rate was 1°/min and no internal standard was required. The sum of the accumulated counts was recorded every 0.1° in 2θ and the integrated relative intensities were obtained by summing under the peak and subtracting off the background averaged over five points on either side of the peak. No attempt was made to resolve overlapping reflections. The refinement program weights the intensities by their relative errors, which are given by

$$\delta(I) = \sqrt{I_T + N \cdot \bar{b}},$$

where I_T is the total sum of the counts of the N points under the peak and $\bar{b}$ is the average background.

It was shown in the preceding section that the X-ray structure factor of a reflection described by the Miller indices, hkl, is given by,

$$S_{hkl} = \sum_{j=1}^{n} f_j \exp[2\pi i(hx_j + ky_j + lz_j)]\exp(-B_j \sin^2\theta/\lambda^2).$$

The intensity of the reflection is proportional to the square of the absolute value of S_{hkl}, and for X-ray diffraction, the relative intensity contains four other factors. These are the multiplicity of the reflection, m, an absorption correction, A_{hkl}, a polarization factor (to account for the effect

of an unpolarized incident beam) and the Lorentz factor, which depends on the diffraction geometry. The polarization factor, $\frac{1}{2}(1 + \cos^2 2\theta)$, and the Lorentz factor, $1/\sin 2\theta$, are generally grouped together as one correction, which is called the Lorentz-polarization factor and is symbolized as L_p. Thus, the calculated relative intensity of an X-ray peak may be expressed as

$$I_{hkl} = m\, A_{hkl}\, L_p\, |S_{hkl}|^2.$$

However, X-ray intensities measured, as in this work, on a diffractometer using a flat plate sample geometry are all reduced by the same absorption factor (Cullity 1956). Thus, the absorption factor has no effect on the relative intensities and therefore can be ignored. The multiplicity of the reflection is the number of planes in the unit cell which have identical interplanar spacings.

3.2.2 Neutron Powder Data

Neutron data were collected over the range $14° \leq 2\theta \leq 108°$ with the position sensitive detector (PSD) described earlier. The neutrons detected over the 35° range of the PSD were sorted into 256 channels according to their position of impact. The counting times were approximately 24 hours per position for the 4 mm sample holder and 12 hours for the 8 mm sample holder. Resolution of partially resolved peaks was accomplished by fitting to an overlapping Gaussian function. The fitting program was largely based on a sub-

routine called Regress (Bevington 1969) which performs a multiple linear regression on data described by a specified function,

$$y = a_o + a_1x_1 + a_2x_2 + \ldots + a_nx_n,$$

which is linear in the coefficients, a_j, to be fitted. The first two terms a_o and a_1x_1 in the function fitted represented a linear fit to the background under the multiple peak, while the subsequent terms represented the contributions of the individual Gaussian peaks. Thus,

$$x_j = \exp - \frac{(u - \bar{u}_j)^2}{2\sigma_j^2}$$

where, for the j^{th} peak, σ_j is the standard deviation of the Gaussian distribution, which is directly related to the peak width, u is the scattering angle, 2θ, and $\bar{u}_j$ is angle of the peak center. The amplitude of the j^{th} peak is then a_j.

The Gaussian peak width is a function of the sample width and the scattering angle, and therefore, can be estimated from the widths of single polycrystalline copper peaks obtained using the same 4 and 8 mm diameter sample holders as were used to collect the original data. The error in the measured intensities is, as in the case of X-ray diffraction, given by,

$$\delta(I) = \sqrt{I_T + N \cdot \bar{b}}.$$

The calculated relative intensity of the reflection (hkl) is represented by an expression analogous to that for

X-ray intensities, except that, since neutrons are uncharged, there is no polarization factor required:

$$I_{hkl} = m\ L\ A_{hkl}\ |S_{hkl}|^2 .$$

where m is the multiplicity of the reflection, L is the Lorentz factor, A_{hkl} is the absorption correction, and S_{hkl} is the neutron structure factor. The absorption factor, A_{hkl}, for neutrons is negligibly small for all the atoms in the materials studied except iridium, which has a linear absorption coefficient of 18 cm^{-1} (Bacon 1962).

3.3 Results

3.3.1 Lattice Parameters

The X-ray powder patterns of the intercalation products, Li_xMO_2 (M = Ru and Ir), are very similar to those of the parent rutile structure metal dioxides, with all of the peaks being shifted and many being split slightly. In the case of both Li_xRuO_2 and Li_xIrO_2, the diffraction peaks can be indexed to an orthorhombic cell in which the deformation of the tetragonal rutile cell by the insertion of lithium is evidenced in a large expansion ($\sim$ 0.5 Å) in the [100] and [010] directions and a smaller contraction ($\sim$ 0.3 Å for $Li_{0.9}RuO_2$ and $\sim$ 0.05 Å for $Li_{0.9}IrO_2$) along the [001] axis. The lattice parameters of this orthorhombic phase for the series Li_xRuO_2 and Li_xIrO_2 are given in Tables 3.1 and 3.2 respectively. No significant variation in the cell parameters of the orthorhombic phase is observed over the compositions studied.

Table 3.1

Lattice Constants for the Orthorhombic Phase in Materials of Composition Li_xRuO_2

$x \pm 0.5$	a (Å)	b (Å)	c (Å)	Vol ($Å^3$)
0	4.4930(20)		3.1050(20)	62.68(10)
.15[a]	5.066	4.966	2.776	
.26[a]	5.066	4.966	2.776	
.52	5.0588(40)	4.9614(42)	2.7789(24)	69.75(17)
.54	5.0700(41)	4.9696(43)	2.7751(27)	69.93(19)
.86	5.0618(31)	4.9667(36)	2.7713(35)	69.67(18)
1.20[b]	5.0729(31)	4.9662(29)	2.7809(37)	70.06(18)
ave	5.066 (36)	4.966 (38)	2.776 (31)	

[a]Too few peaks from the orthorhomibc phase were present in these lower compositions to fit the cell parameters, but the observed peaks are reasonably well (±0.08°) described by the average cell parameters.

[b]Subsequent re-analysis of this sample by atomic absorption revealed that it is actually $Li_{0.87}RuO_2$.

Values in parentheses are estimated standard deviations referring to the least significant digit(s).

Table 3.2

Lattice Constants for the Orthorhombic Phase in Materials of Composition Li_xIrO_2

x ± 0.5	a (Å)	b (Å)	c (Å)	Vol (Å^3)
0	4.4987(13)		3.1552(27)	63.86(9)
0.28	4.9678(36)	4.7573(41)	3.1034(38)	73.34(21)
0.37	4.9607(28)	4.7592(26)	3.0975(51)	73.13(20)
0.64	4.9701(42)	4.7591(38)	3.1074(45)	73.50(23)
0.87	4.9615(41)	4.7579(36)	3.1084(59)	73.38(26)
0.88	4.9688(39)	4.7573(38)	3.1063(54)	73.43(24)

Values in parentheses are estimated standard deviations referring to the least significant digit(s).

Nominal compositions of Li_xMO_2 (M = Ru and Ir) with $x \lesssim 0.7$ have peaks assignable to MO_2 reflections in their X-ray powder patterns indicating that they are mixtures of the limiting compositions, $Li_{.9}MO_2$ and MO_2, rather than one single non-stoichiometric phase.

The study of Li_xOsO_2 proved to be a difficult problem since the metal dioxide host, OsO_2 has two rutile phases with quite similar lattice parameters (Bowman 1970b) and (Ryabov et al 1968). As a result, the X-ray powder diffraction peaks of Li_xOsO_2 were broadened due to overlapping to such an extent that determination of the lattice parameters was not possible.

3.3.2 RuO_2 Structure Refinement

As a test of the position sensitive detector and the structure refinement procedure, a neutron data set was collected and refined for RuO_2, whose structure is accurately known (Bowman 1970). The absence of all reflections (0kl) with $k + l \neq 2n$ (for integral n) in both the X-ray and neutron powder diffraction pattern was consistent with the rutile space group, $P4_2/mnm$ (#136). The results of the refinement (Table 3.3) are in good agreement with the single crystal X-ray refinement of the structure (Bowman 1970a).

3.3.3 Li_xRuO_2 Structure Refinement

X-ray and neutron diffraction data were collected for two different preparations of Li_xRuO_2, which originally analysed to 0.86 and 1.20 moles of lithium per mole RuO_2.

Table 3.3

Structural Parameters from Refinement of

Neutron Powder Data for RuO_2

		Powder[a] 1.40 Å	Crystal[b] MoKo
Ru	X	0.0	0.0
	Y	0.0	0.0
	Z	0.0	0.0
	B(Å^2)	-0.02(20)	0.384(12)
O	X	0.305(1)	0.3058(16)
	Y	0.305(1)	0.3058(16)
	Z	0.0	0.0
	B(Å^2)	0.22(20)	0.517(8)
	R	5.81	-
	R_w	8.40	-
#I's		23	-
#hkl's		27	235

[a] Space group $P4_2/mnm$. Scattering lengths taken as 0.73 and 0.58×10^{-12} cm for Ru and O respectively (Koester 1977). Values in parentheses are estimated standard deviations referring to the least significant digit(s).

[b] Structural parameters obtained from a previous single crystal X-ray study (Bowman 1970a).

$Li_{1.2}RuO_2$ was of particular interest because there is only one available octahedral site per metal ion and therefore, it was expected that some or all of the cations must be four-coordinated.

Five systematic absences were observed in both the X-ray and neutron data: (0kl) for $k + l \neq 2n$, (h0l) for $h + l \neq 2n$, (h00) for $h \neq 2n$, (0k0) for $k \neq 2n$ and (001) for $l \neq 2n$ where n is an integer. These absences are consistent with only two orthorhombic space groups, Pnnm (#58) and its acentric counterpart, Pnn2 (#34); the centric group was chosen for the initial refinement. The orthorhombic space group Pnnm is a lower symmetry subgroup of the tetragonal rutile space group, $P4_2/mnm$, obtained by removal of the 4_2 screw axis. Consequently, similar sites are found in the two groups. In rutile structure RuO_2, the metal atoms and anions occupy the a-site at 0,0,0 and the f-site at x,x,0 respectively. The initial trial sites chosen for the refinement of the ruthenium and oxygen positions in Li_xRuO_2 were the a-site of Pnnm at 0,0,0 and the g-site of x,y,0 respectively. The X-ray powder diffraction data refined for only one of the two preparations of Li_xRuO_2, the one which was nominally $Li_{1.2}RuO_2$. Even though the sample had been ground up finely, the intensities of the $Li_{.86}RuO_2$ sample not only did not refine but were not reproducible. This suggests that the material is subject to preferred orientation, which was probably enhanced by pressing the sample into a grooved glass

slide to obtain the diffraction pattern.

From a refinement based on 15 X-ray intensities (Table 3.4), it was found that the Ru atoms occupy the a-site at 0,0,0 and the oxygen atoms occupy the g-site at 0.237(15), 0.360(38), 0.0 as predicted. The negative temperature factors are probably a consequence of poor statistics; five parameters were refined with only fifteen intensities.

Refinement of the neutron intensities of both preparations of Li_xRuO_2 yielded the same Ru and O positions (within the limits of error) as were found from the X-ray data. However, as mentioned previously, neutron diffraction is sensitive to the position of the lithium atoms as well as to those of the heavy atoms. In the first chapter, it was shown that the most probable sites for lithium are in the vacant channels between the chains of octahedrally coordinated transition metal atoms. In the space group Pnnm there are three sites which correspond to positions in these channels. One of them is a site of multiplicity 4 at $0\frac{1}{2}z$, in which lithium would be approximately tetrahedrally coordinated by oxygen if $z = \frac{1}{4}$, and the other two are sites of multiplicity 2 at $0\frac{1}{2}\frac{1}{2}$ and $0\frac{1}{2}0$, in which lithium is approximately octahedrally coordinated by oxygen. Refinements of the structures, for both preparations of Li_xRuO_2, were attempted with all of the lithium in each of these three sites and with the lithium divided in various ratios over all possible combinations of two of these sites. Though the data of $Li_{.86}RuO_2$ refined

Table 3.4

Structural Parameters from Refinement of

Powder Data for $Li_{0.9}RuO_2$

		$Li_{0.87}RuO_2$		$Li_{0.86}RuO_2$
		X-ray 1.54 Å	Neutron 1.40 Å	Neutron 1.40 Å
Ru	X	0.0	0.0	0.0
	Y	0.0	0.0	0.0
	Z	0.0	0.0	0.0
	B($Å^2$)	-0.10(29)	0.31(35)	0.95(22)
O	X	0.240(13)	0.2555(40)	0.2501(26)
	Y	0.356(35)	0.3365(44)	0.3316(35)
	Z	0.0	0.0	0.0
	B($Å^2$)	-1.3(2.0)	0.09(26)	0.37(15)
Li	X	-	0.0	0.0
	Y	-	0.5	0.5
	Z	-	0.5	0.5
	B($Å^2$)	-	2.7(2.0)	0.32(76)
R		7.6	9.62	8.13
R_w		9.18	10.24	7.22
#I's		15	21	21
#hkl's		36	58	73

Neutron scattering lengths taken as -0.203, 0.73, and 5.8×10^{-12} cm for Li, Ru and O respectively (Koester 1977). Values in parentheses are estimated standard deviations referring to the least significant digit(s).

readily (Appendix I), refinement of the data from the sample nominally $Li_{1.20}RuO_2$ placed a large portion of the lithium in a site which was too small for Li^+. A re-analysis of the lithium content of the material by atomic absorption revealed that the composition was actually $Li_{.87}RuO_2$. A reasonable refinement of the data was obtained with the new x value (Appendix I). The best fits to the observed intensities were obtained with all of the lithium in either the 0½½ site or in the 0½z site. In both these sites, the refinement resulted in an R-value close to the mean relative error in the intensities ($\sim$ 8%) indicating acceptable agreement between the observed and calculated intensities. However, in the case of the 0½z site, the z parameter refined to ½ (within error) and therefore, this site is 6-coordinated and can be no more than half-filled to allow adequate separation between the lithium atoms. This is not a problem since $x < 1$ for both of the preparations of Li_xRuO_2 studied and consequently, the 0½z site would be less than half-filled. However, since the R_w-factors of the two refinements are only slightly different (7.22 and 7.21 for Li at 0,½,½ and at 0,½,0.48(7), respectively, in the case of $Li_{.86}RuO_2$), the 0½z site with its extra degree of freedom is not a significant improvement over the special site at 0½½ (Hamilton 1965).

The results of the structure refinements for the two preparations of Li_xRuO_2 (Table 3.4) are in acceptable agreement with each other, as expected since their compositions

are not significantly different.

3.3.4 Li_xIrO_2 Structure Refinement

X-ray and neutron diffraction data were collected for the Li_xIrO_2 sample of nominal composition $Li_{.87}IrO_2$. All the observed X-ray peaks were assignable to an orthorhombic cell and the systematic absences were the same as those observed for $Li_{.9}RuO_2$. Refinements of the X-ray data for several preparations of Li_xIrO_2, with different nominal lithium compositions, in the space group P_{nnm} always resulted in unreasonable oxygen positions and an R-value no less than 16%.

The neutron data collected for $Li_{.87}IrO_2$ has a medium sized peak, corresponding to d = 1.924 Å, which could not be explained in terms of the orthorhombic cell determined from the X-ray data or by doubling any one or two of the cell edges. All attempts to find a monoclinic cell which could explain the observed reflections were unsuccessful. The peak at d = 1.924 Å can, however, be ascribed to the (200) reflection of iridium metal. Since the IrO_2 used for the intercalation was prepared by oxidizing iridium metal, it is possible that some unoxidized metal may be present in the sample. The facts that the Ir peak was not observed in the X-ray diffraction pattern of the same sample and that neutrons have a greater penetration depth than X-rays suggests that the Ir metal is only or mostly present in the cores of the particles. This is not an unreasonable hypothesis, since a problem with sintering was encountered in the preparation

of IrO_2.

As a result, all the peaks which could have contributions from Ir metal were removed from the data for the structure refinement. The intensities were also corrected for absorption (Bacon 1962). Even after these corrections, it was impossible to refine the data to an R-value less than 30%.

The X-ray diffraction intensities of IrO_2 (whose structure is accurately known), obtained before intercalation, also did not refine and were not reproducible. It is reasonable to suspect, therefore, that preferred orientation is a problem in these materials. The IrO_2 crystals grown for this work were largely needle-like and very hard, and therefore, quite difficult to grind up finely. The refinement program used, MARYSE (L'Helgoualch et al 1977), is capable of handling preferred orientation for plate-like crystals only, and so, it is not surprising that all attempts to refine the preferred orientation parameter were unsuccessful.

CHAPTER 4

DISCUSSION

In samples of both Li_xRuO_2 and Li_xIrO_2 of low nominal lithium content peaks assignable to the host dioxide were present in the powder diffraction patterns. This fact indicates that at least for the compositions studied ($0.2 \lesssim x \lesssim 0.9$) both Li_xRuO_2 and Li_xIrO_2 are two phased systems. Therefore, rather than having one nonstoichiometric phase over the range of lithium compositions, as in the case of Li_xTiS_2 (Dahn et al 1980), compounds nominally Li_xRuO_2 and Li_xIrO_2 are mixtures of their limiting compositions, $Li_{.9}MO_2$ and MO_2. A wide two phase region has also been observed in a related compound, Li_xMoO_2 (Di Salvo et al 1979/80). This feature, however, makes these systems less suitable candidates for use as solid state cathodes, because the rate of intercalation (or cell discharge) and the reversibility of the reaction are likely to be slower than that of a material which is nonstoichiometric over a wide range of x, and where consequently, no nucleation of a new phase is required.

The two phase system suggests that there is large local strain associated with the insertion of lithium into the rutile host. A comparison of the bonding in RuO_2 with that in $Li_{.86}RuO_2$ and $Li_{.87}RuO_2$ (Table 4.1) reveals that a

Table 4.1

Interatomic Distances and Angles in RuO_2, $Li_{.86}RuO_2$ and $Li_{.87}RuO_2$ from Refinement of Neutron Powder Data

	RuO_2	$Li_{.86}RuO_2$	$Li_{.87}RuO_2$
Ru-O octahedron			
Distance	4 at 1.988(3) 2 at 1.935(4)	4 at 2.054(11) 2 at 2.077(16)	4 at 2.032(15) 2 at 2.115(21)
Angle			
O_1-Ru-O_2	180.0(2)	180.0 (7)	180.0(10)
-O_3	102.7(1)	84.8 (4)	86.3(6)
-O_4	77.3(1)	95.2 (4)	93.7(6)
-O_5	90.0(1)	87.0 (5)	86.7(7)
-O_6	90.0(1)	93.0 (5)	93.3(7)
O_3-Ru-O_5	90.0(1)	87.0 (5)	86.7(7)
Li-O octahedron			
Distance	- -	4 at 2.055(11) 2 at 2.077(16)	4 at 2.067(15) 2 at 2.081(21)
Angle			
O_1'-Li-O_2'	-	180.0 (7)	180.0(10)
-O_3'	-	84.8 (4)	84.5(5)
-O_4'	-	95.2 (4)	95.5(5)
-O_5'	-	87.0 (5)	86.7(7)
-O_6'	-	93.0 (5)	93.3(7)
O_3'-Li-O_5'	-	87.0 (5)	86.7(7)

substantial expansion of the oxygen octahedron accompanies the incorporation of lithium. The bond lengths of octahedrally coordinated Li in $Li_{.9}RuO_2$ are comparable with those of octahedrally coordinated Li in $LiNbO_3$ at 2.068(11) and 2.238 (23) Å (Abrahams et al 1966) and in $LiReO_3$ at 2.000(6) and 2.42(1) Å (Cava et al 1982). However, the coordination of lithium in $Li_{.9}RuO_2$ is more regular than in either of these compounds or that observed in $LiMoO_2$ where the Li-O bond lengths vary from 2.04(2) to 2.20(2) Å (Cox et al 1982).

Though $Li_{.9}RuO_2$ has a c/a ratio (0.548) close to that for ideal tetragonal close packing (0.586) (Baur 1981), the lithium atoms do not occupy 4-coordinated sites as Baur had predicted they might. However, it was still possible that the data might refine with all the cations, including the Ru, in tetrahedral sites, as in Li_4GeO_4. In the channels occupied by Ru, the 4-coordinated sites are located at 00¼, 00¾, ½½¼ and ½½¾, while the 4-coordinated sites in the other channel, presumably occupied by lithium, are at 0½¼, 0½¾, ½0¼ and ½0¾. Using these initial positions and assuming random ordering of the Ru and Li atoms in their respective channels, the oxygen positions and the cation z coordinate were allowed to refine. The weight R-value (35%) resulting from the refinement clearly indicated that this model was not a reasonable fit to the diffraction data; $Li_{.9}RuO_2$ does not adopt a Li_4GeO_4-type structure.

Since there is only one available octahedral site per

transition metal ion to accommodate Li^+, lithium ions in Li_xRuO_2 if $x > 1$ must occupy other sites. If the lithium ions occupy the same channels as in $Li_{.9}RuO_2$ and there is no significant expansion of the c-axis, then, assuming a crystal radius of 0.73 Å (Shannon 1976), the lithium ions must occupy the site at 0½z with $z = 0.25$. In $Li_{.9}RuO_2$ the radius of this site is only 0.36 Å. Consequently, a radical change in structure must be expected if $x > 1$. Baur pointed out that it is possible to fill 25% more tetrahedral interstices than there are close packed atoms without sharing faces between coordination tetrahedra in tetragonal close packing (Baur 1981), making possible such structures as Li_4GeO_4. In Li_xRuO_2 with $x > 1$ there are more cations than close packed anions and thus, a Li_4GeO_4-type structure with tetrahedral coordination of all the cations might be favourable.

The structure of $LiMoO_2$ from neutron powder diffraction was reported after this work was almost completed (Cox et al 1982). In that publication, the similarity between the structure of $LiMoO_2$ and NiAs structure was pointed out (Table 4.2). The authors stated that they belived $LiMoO_2$ to be the first oxide known to have a distorted NiAs-type structure.

$Li_{.9}RuO_2$ can also be regarded as a distorted NiAs-type compound. In Figure 4.1 the solid line represents the rutile cell and the broken line, the basic NiAs-like cell, which is not quite hexagonal with $a = 2.844$ Å, $b = 2.771$ Å and $\gamma = 119.2°$. The relationship between rutile and NiAs

Table 4.2

Comparison of Structural Parameters from Rietveld Refinement of Neutron Powder Data for $Li_{0.98}MoO_2$ with Values Based Upon an Ideal NiAs-Type Structure.

(From Cox et al 1982)

		1.43 Å 295 K	Ideal NiAs
Mo	X	0.2243(5)	0.25
	Y	-0.0041(14)	0
	Z	0.0063(7)	0
	B(Å^2)	0.25(5)	-
O(1)	X	0.0904(9)	0.0833
	Y	0.2613(7)	0.25
	Z	0.1832(7)	0.1667
	B(Å^2)	0.11(9)	-
O(2)	X	0.4111(9)	0.4167
	Y	0.7349(8)	0.75
	Z	0.3319(8)	0.3333
	B(Å^2)	0.17(10)	-
Li	X	0.260(2)	0.25
	Y	0.000(5)	0
	Z	0.514(3)	0.5
	B(Å^2)	0.7(2)	-
	a(Å)	5.5654(4)	-
	b(Å)	5.2086(4)	-
	c(Å)	5.8587(5)	-
	β(deg)	118.765(5)	-
	Vol(A^3)	148.88(3)	-
	R_I	0.029	-
	R_{WP}	0.116	-
	R_E	0.097	-

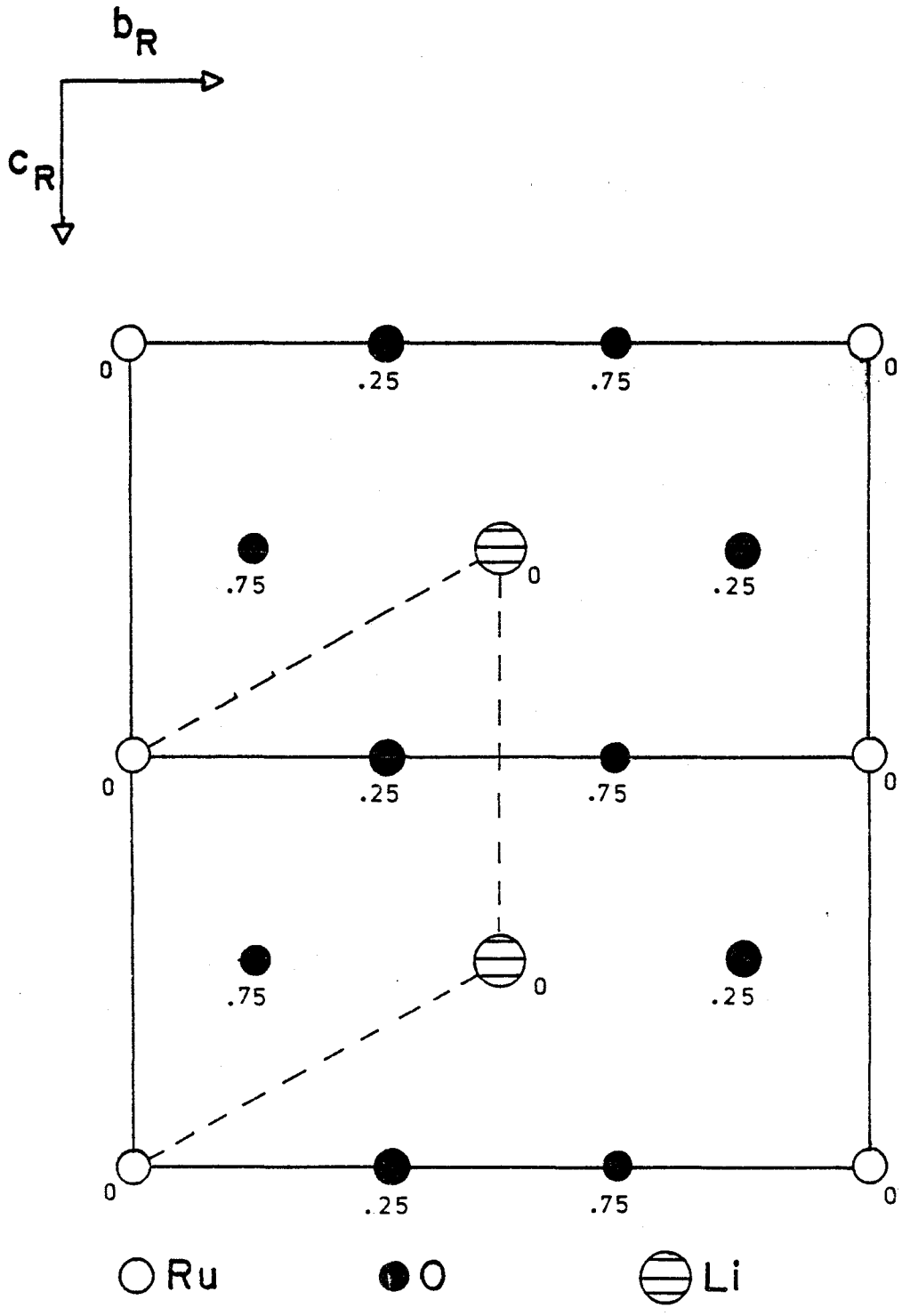

Figure 4.1 Projection of $Li_{0.9}RuO_2$ structure on (100) plane. The rutile cell is shown in heavy outline and the distorted NiAs cell with broken lines. The numbers denote the fractional coordinates along the a direction.

structure has been described by (Wells 1962) and is depicted in Figure 4.2. NiAs structure (Fig. 4.2(a)) is formed from a hexagonal close packed lattice of anions with cations filling all the octahedral interstices. In the rutile structure (Fig. 4.2(b)) only one-half of the octahedral sites are occupied and the close packed layers of anions are buckled to make three oxygens coplanar with the nearest cation. In an ideal NiAs cell the cations are located at 000 and 00½ and the anions, at ⅓ ⅔ ¾ and ⅔ ⅓ ¼. When transformed to the orthorhombic cell of $Li_{.86}RuO_2$, the cation sites become the observed positions of Ru and Li at 000 and 0½½ respectively, while the anion sites become the observed positions of oxygen at ¼⅓ 0 and ¾ ⅙ ½ (Table 4.3). A comparison of Tables 4.2 and 4.3 reveals that $Li_{.9}RuO_2$ bears a closer resemblance to an ideal NiAs structure than even $LiMoO_2$, making $Li_{.9}RuO_2$ the second oxide reported to have a distorted NiAs structure.

It is perhaps interesting to note that though MoO_2 is a distorted rutile with monoclinic symmetry, the intercalation products of both MoO_2 and RuO_2 (an undistorted rutile) are quite similar. This suggests that crystallographic distortions have no serious effect on lithium intercalation in rutile related transition metal dioxides.

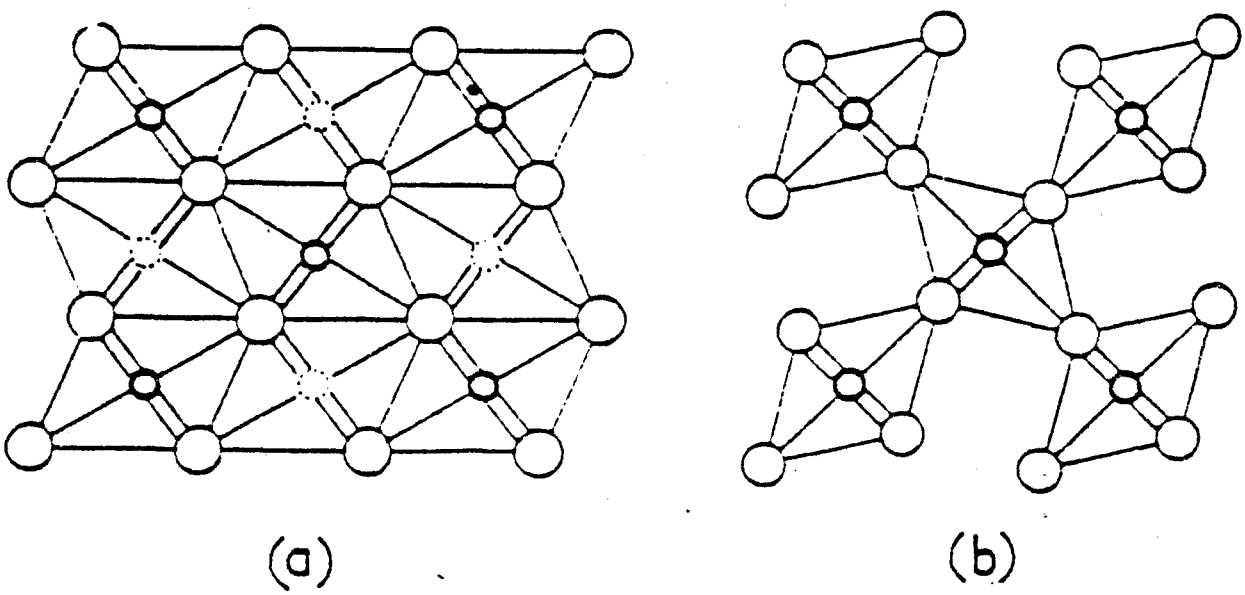

Figure 4.2 Relationship between rutile and NiAs structure (from Wells 1962). In NiAs structure (a) the anions are in regular hexagonal close packing and all the octahedral interstices are filled. The anions in rutile structure (b) are puckered to make the three neighbouring oxygens coplanar with the cations occupying one half of the octahedral interstices.

Table 4.3

Comparison of Structural Parameters

from Refinement of Neutron Powder Data for $Li_{0.86}RuO_2$

with Values Based Upon an Ideal NiAs-Type Structure

		$Li_{0.86}RuO_2$	Ideal NiAs
Ru	X	0.0	0.0
	Y	0.0	0.0
	Z	0.0	0.0
O	X	0.2501(26)	0.250
	Y	0.3316(35)	0.333
	Z	0.0	0.0
Li	X	0.0	0.0
	Y	0.5	0.5
	Z	0.5	0.5

CHAPTER 5

CONCLUSIONS

In summary, it is found that both Li_xRuO_2 and Li_xIrO_2 have orthorhombic unit cells which are related to the host tetragonal rutile cell by a substantial ($\sim$ 0.5 Å) expansion along the a and b axes and a smaller contraction along the c axis. These systems have a wide two phased region rather than a single nonstoichiometric phase over the range of compositions studied ($.2 \lesssim x \lesssim .9$), and therefore, are probably not good candidates for use in secondary batteries.

The structural study of $Li_{.9}RuO_2$ revealed that all the cations are in octahedral rather than tetrahedral coordination. $Li_{.9}RuO_2$ adopts a NiAs-type structure very similar to that reported for $LiMoO_2$ (Cox et al 1982).

A different type of structure must be expected for Li_xRuO_2 if $x > 1$. Thus, a systematic study of the effects of temperature, solution concentration, and time on lithium uptake, with the aim of finding route to maximizing the lithium content of the product, would be quite valuable, and might verify whether or not $Li_{1.3}RuO_2$, as reported by (Murphy et al 1978), can really be prepared.

IrO_2 and OsO_2 were also reported to incorporate as much as 1.5 Li per MO_2 molecule (Murphy et al 1978) and

consequently, further work on these compounds would certainly be worthwhile. The problem of preferred orientation in Li_xIrO_2 might be alleviated by fitting an appropriate preferred orientation factor in the structure refinement, or by adding an inert material with desirable scattering properties to the sample to help randomize the particle orientations.

Single phased OsO_2 might be produced from a different preparative procedure. The initial product of the gas transport crystal growth, described in the experimental chapter, had very sharp diffraction peaks, indicating that it was single phased, and a brilliant golden colour. After several days, the sample tarnished to a dark brown colour and the lines in the diffraction pattern showed splitting, signifying the presence of a second phase. All the observed lines were assignable to the two known rutile phases of OsO_2.

This suggests that the product of the gas transport growth is a kinetic or metastable phase, perhaps due to some of the structural features of the transporting gas, OsO_4, remaining in the deposited OsO_2 crystals. A growth procedure not involving gas transport might therefore produce a single phased product. Alternatively, if the product of the gas transport reaction is left for an adequate period of time, then perhaps it will all convert to the more stable phase, making a study of its intercalation products possible.

REFERENCES

Abrahams, S.C., Reddy, J.M. and Bernstein, J.L., J. Phys. Chem. Solids 27, 997 (1966).

Adams, D.M., Inorganic Solids, Wiley and Sons, London, 1974.

Ashcroft, N.W. and Mermin, N.D., Solid State Physics, Saunders College, Philadelphia, 1976.

Bacon, G.E., Neutron Diffraction, 2nd ed., Clarendon, Oxford, 1962.

Baur, W.H., Mat. Res. Bull. 16, 339 (1981).

Bevington, P.R., Data Reduction and Error Analysis for the Physical Sciences, McGraw-Hill, New York, 1969.

Bowman, C.E., Acta Chem. Scand. 24, 117 (1970).

Bowman, C.E., Acta Chem. Scand. 24, 123 (1970).

Cava, R.J., Santoro, A., Murphy, D.W., Zahurak, S. and Roth, R.S., J. Solid State Chem. 42, 251 (1982).

Cox, D.E., Cava, R.J., McWhan, D.B. and Murphy, D.W., J. Phys. Chem. Solids 43, 657 (1982).

Cullity, B.D., Elements of X-ray Diffraction, Addison-Wesley, London, 1956.

Dahn, J.R., McKinnon, W.R., Haering, R.R., Buyers, W.J.L. and Powell, B.M., Can. J. Phys. 58, 207 (1980).

Dines, M.B., Mat. Res. Bull. 10, 287 (1975).

Di Salvo, F.J., Murphy, D.W. and Waszczak, J.V., Syn. Metals 1, 29 (1979/80).

Hamilton, W.C., Acta Cryst. 18, 502 (1965).

Ikeda, H., Saito, T. and Tamura, H., Manganese Dioxide Symp. Proc. 1, 384 (1975).

Kittel, C., Introduction to Solid State Physics, 5th ed., Wiley and Sons, New York, 1976.

Koester, L., Neutron Physics, Springer Tracts in Modern Physics, Vol. 80, Springer-Verlag, New York, 1977.

L'Helgoualch, H.,Fonteneau, G., Pannetier, J. and Denes, G., Maryse: A Powder Crystal Structure Refinement Program, (unpublished program), 1977.

Murphy, D.W., Di Salvo, F.J., Carides, J.N. and Waszczak, J.V., Mat. Res. Bull. 13, 1395 (1978).

Murphy, D.W. and Christian, P.A., Science 205, 651 (1979).

Murphy, D.W., Christian, P.A., Di Salvo, F.J. and Carides, J.N., J. Electrochem. Soc. 126, 497 (1979).

Rogers, D.B., Butler, S.R. and Shannon, R.D., J. Inorg. Syn. 13, 135 (1971).

Rowe, J.M., Ph.D. Thesis, McMaster University, Hamilton, 1966.

Ryabov, A.N., Semenov, I.N. and Kozhina, I.I., Russian J. Inorg. Chem. 13, 887 (1968).

Shannon, R.D., Acta Cryst. A32, 751 (1976).

Thomas, J.M., Phil. Trans. Roy. Soc. 277, 251 (1974).

Wells, A.F., Structural Inorganic Chemistry, 3rd ed., Clarendon, Oxford, 1962.

Whittingham, M.S. and Dines, M.B., J. Electrochem. Soc. 124, 1387 (1977).

Whittingham, M.S., Prog. Solid St. Chem. 12, 41 (1978).

Woolfson, M.M., An Introduction to X-ray Crystallography, Cambridge University Press, Cambridge, 1970.

Vollenkle, H. and Wittman, A., Z. Krist. 128, 66 (1969).

APPENDIX I

Neutron Diffraction Data of $Li_{0.86}RuO_2$ and $Li_{.87}RuO_2$

The following plots are the raw data obtained from the position sensitive detector. The label $LiRuO_2$(A) stands for $Li_{0.86}RuO_2$ and $LiRuO_2$(B) for $Li_{0.87}RuO_2$. Tables I.1 and I.2 give the observed and calculated neutron diffraction intensities for both samples.

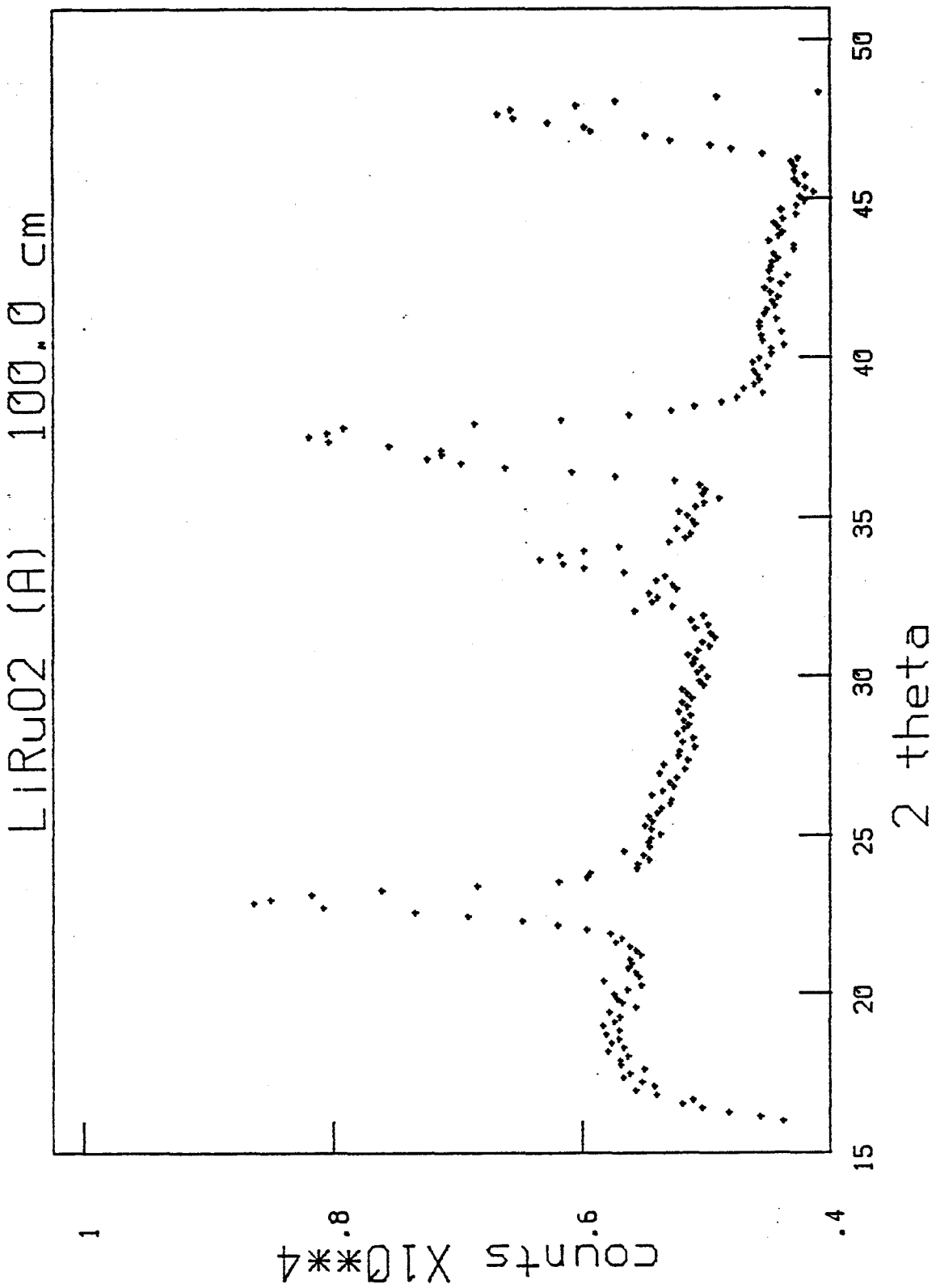
LiRuO2 (A) 100.0 cm
counts X10**4
1
.8
.6
.4
15
20
25
30
35
40
45
50
2 theta

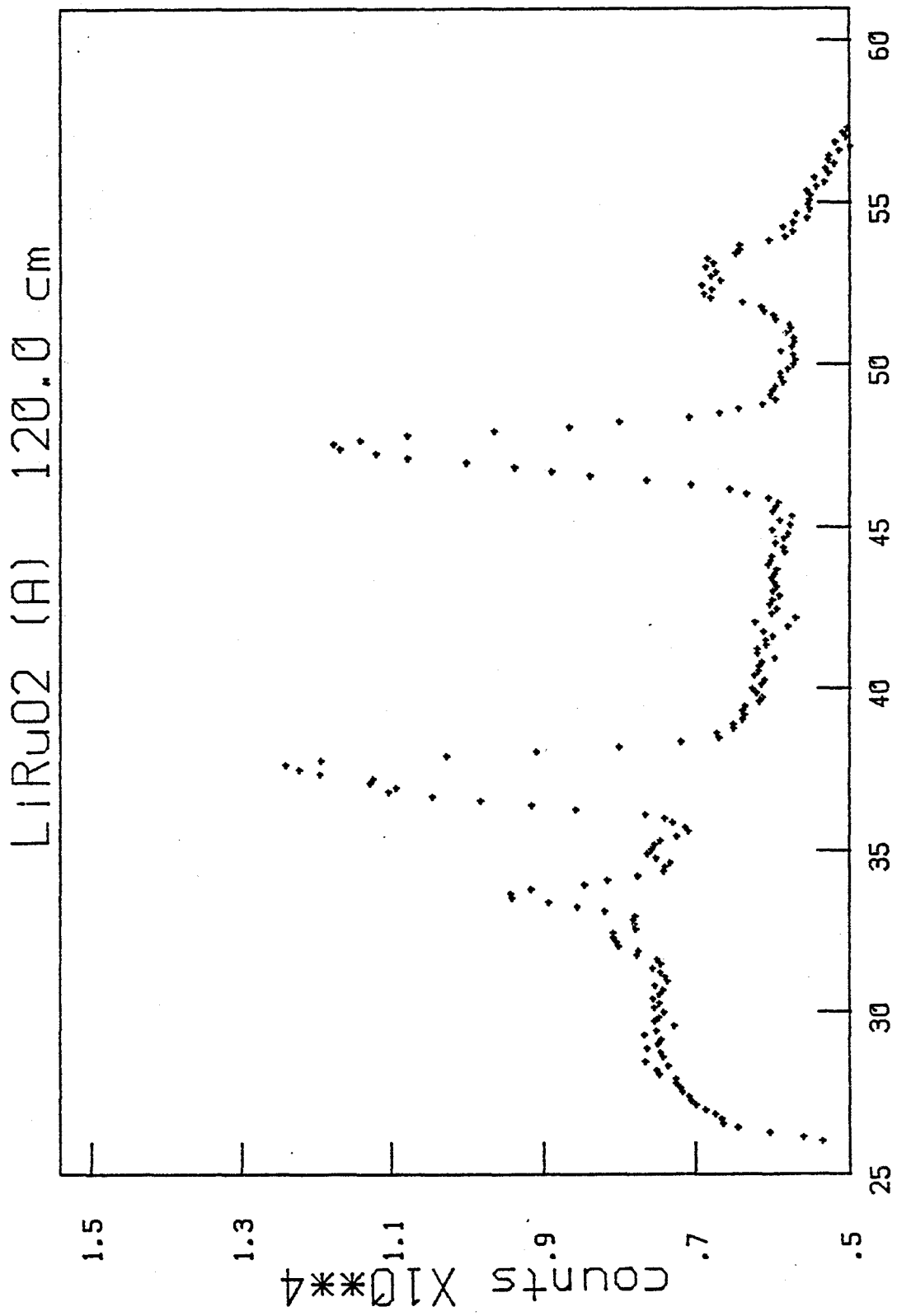
LiRuO2 (A) 120.0 cm
counts X10**4
1.5
1.3
1.1
.9
.7
.5
25
30
35
40
45
50
55
60
2 theta

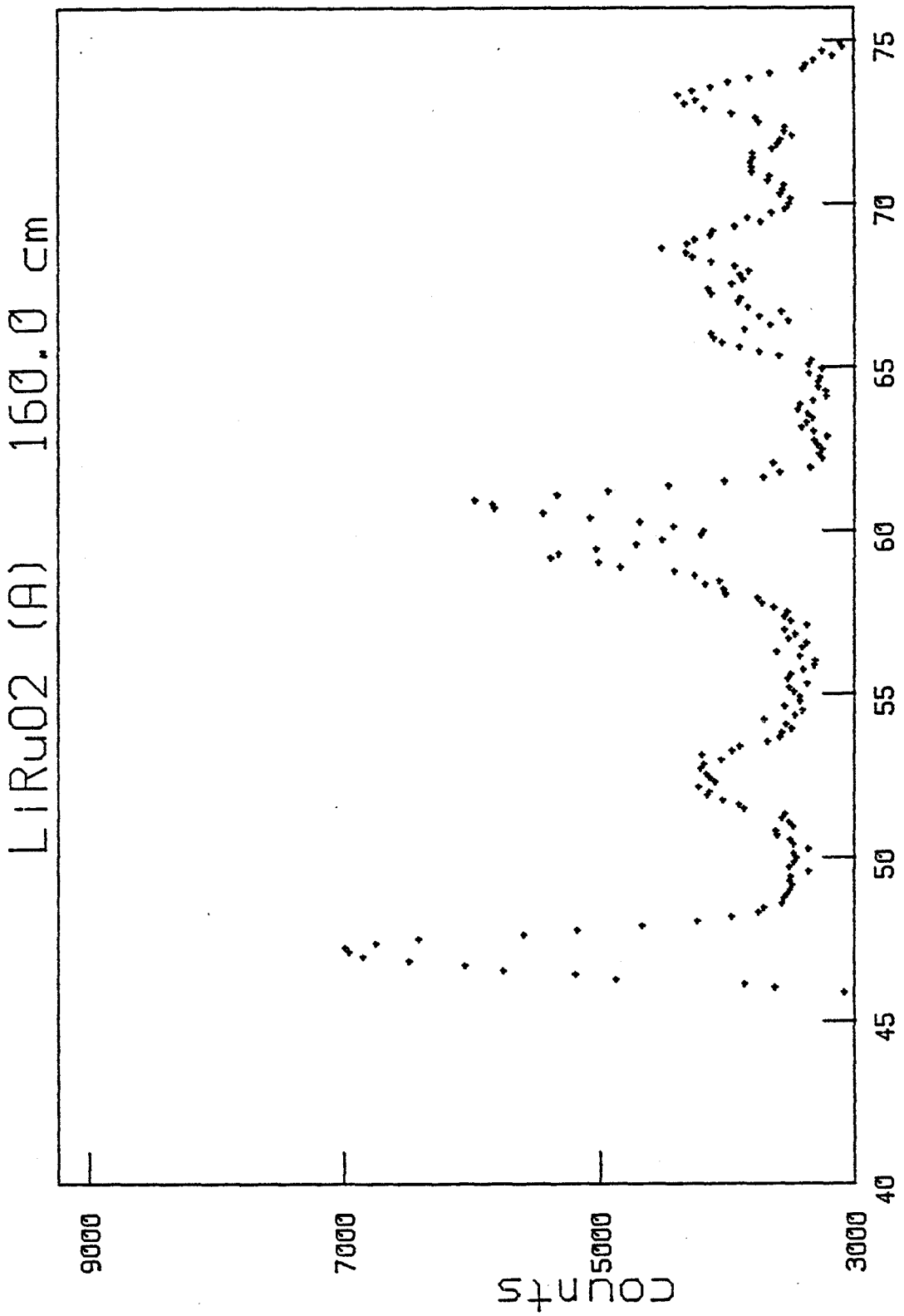
LiRuO2 (A) 160.0 cm
Counts
9000
7000
5000
3000
40
45
50
55
60
65
70
75
2 theta

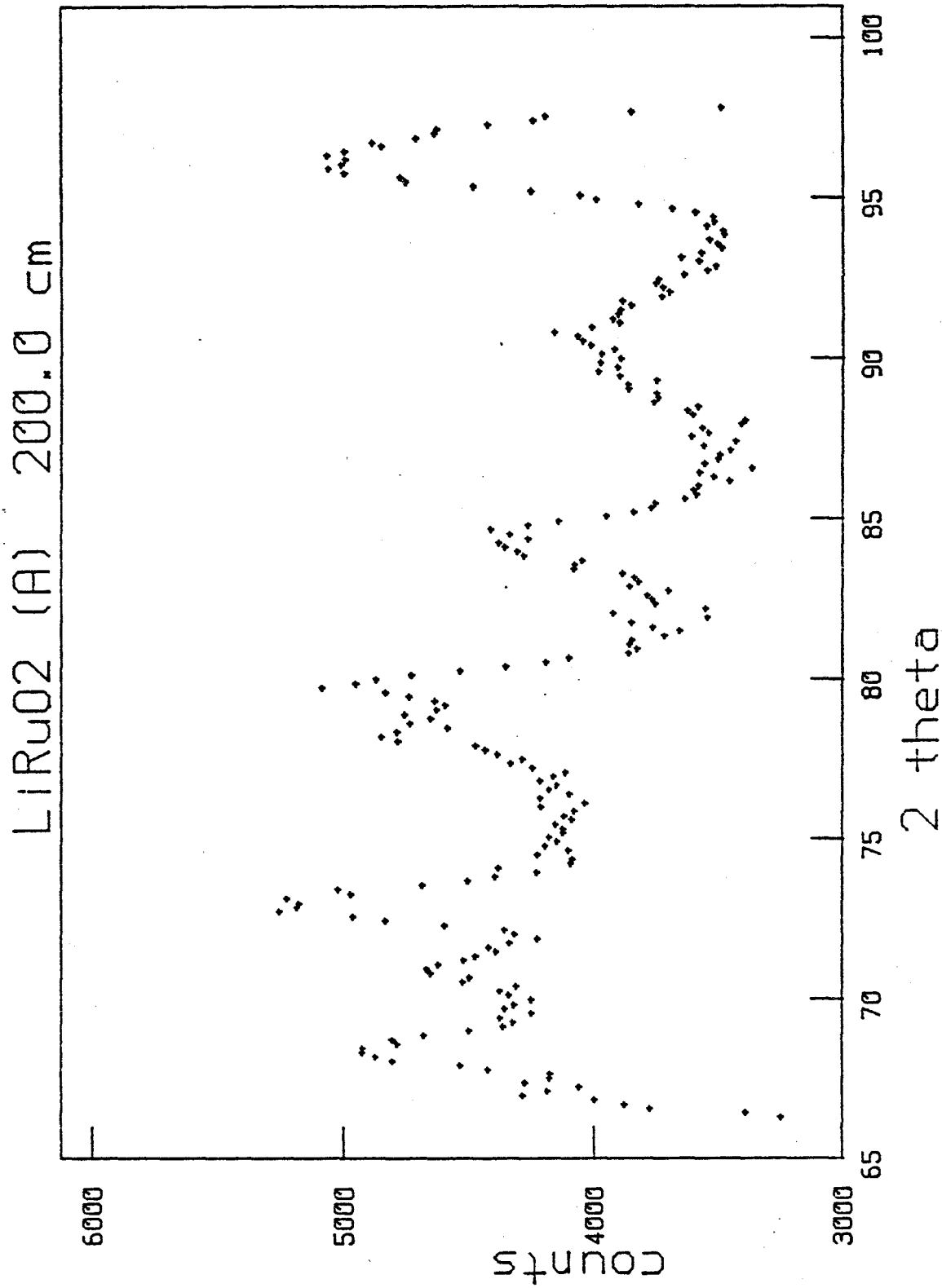
LiRuO2 (A) 200.0 cm
Counts
2 theta
6000
5000
4000
3000
65
70
75
80
85
90
95
100

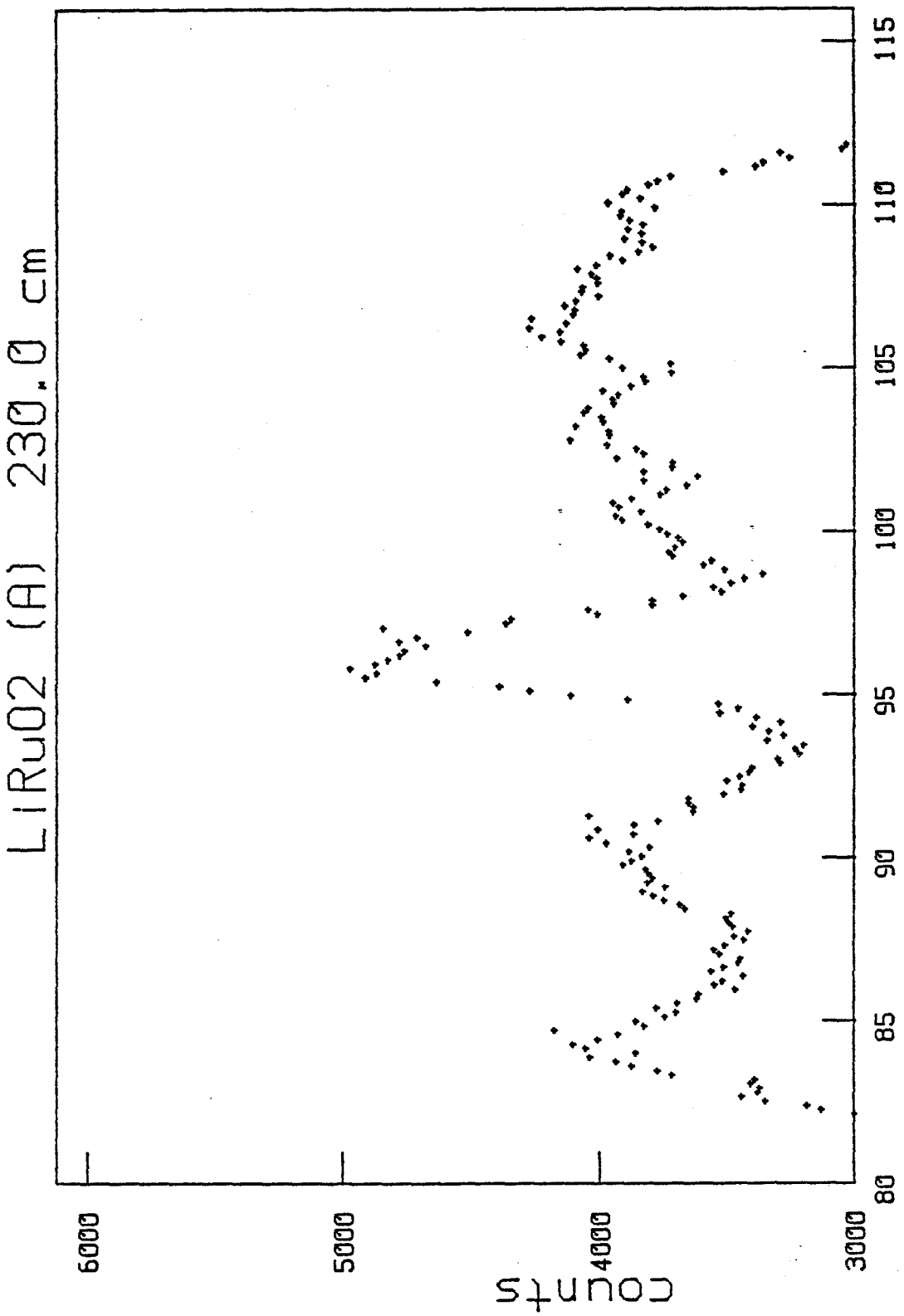
LiRuO2 (A) 230.0 cm
Counts
6000
5000
4000
3000
80
85
90
95
100
105
110
115
2 theta

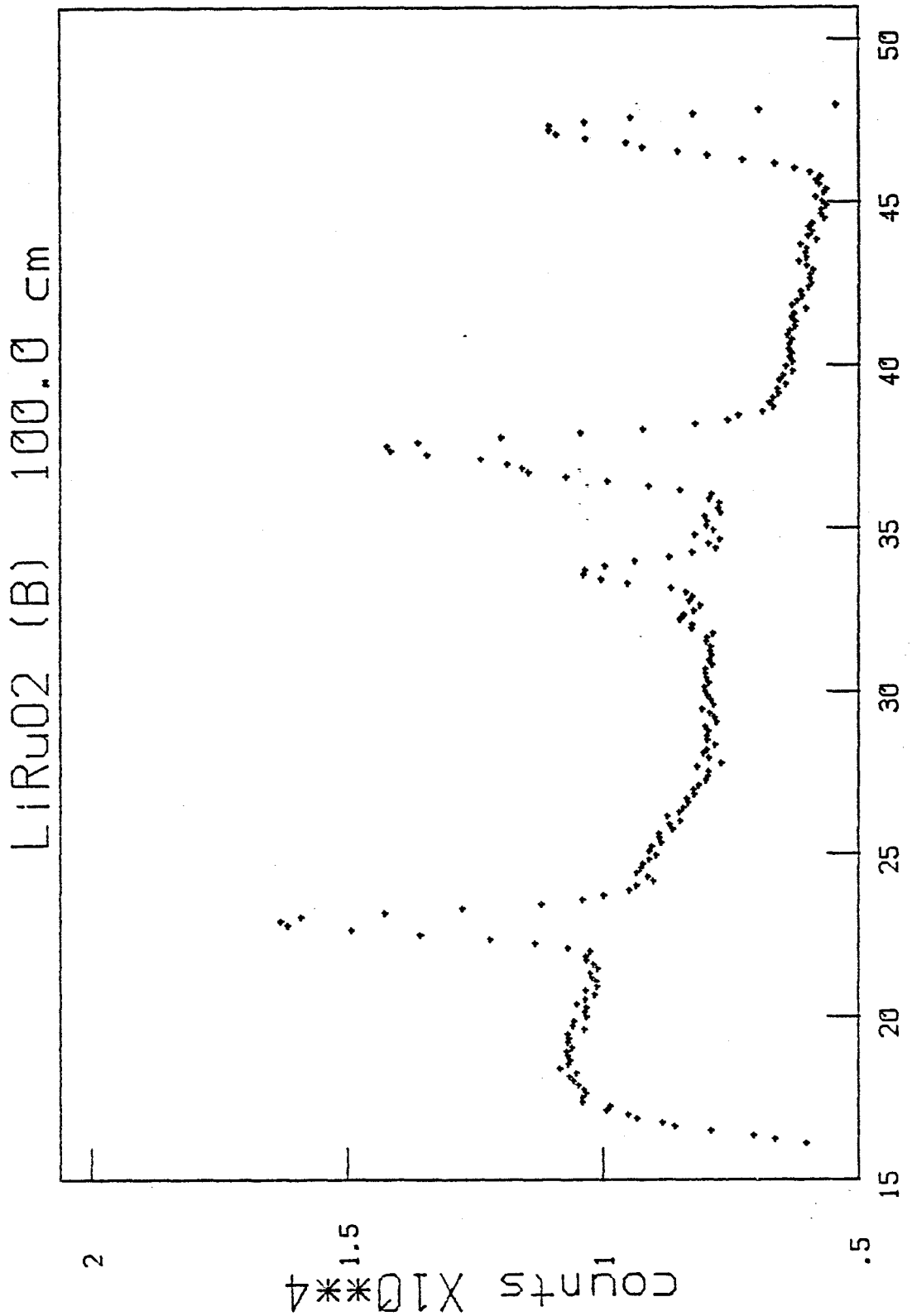
LiRuO2 (B) 100.0 cm
Counts X10**4
2
1.5
.5
15
20
25
30
35
40
45
50
2 theta

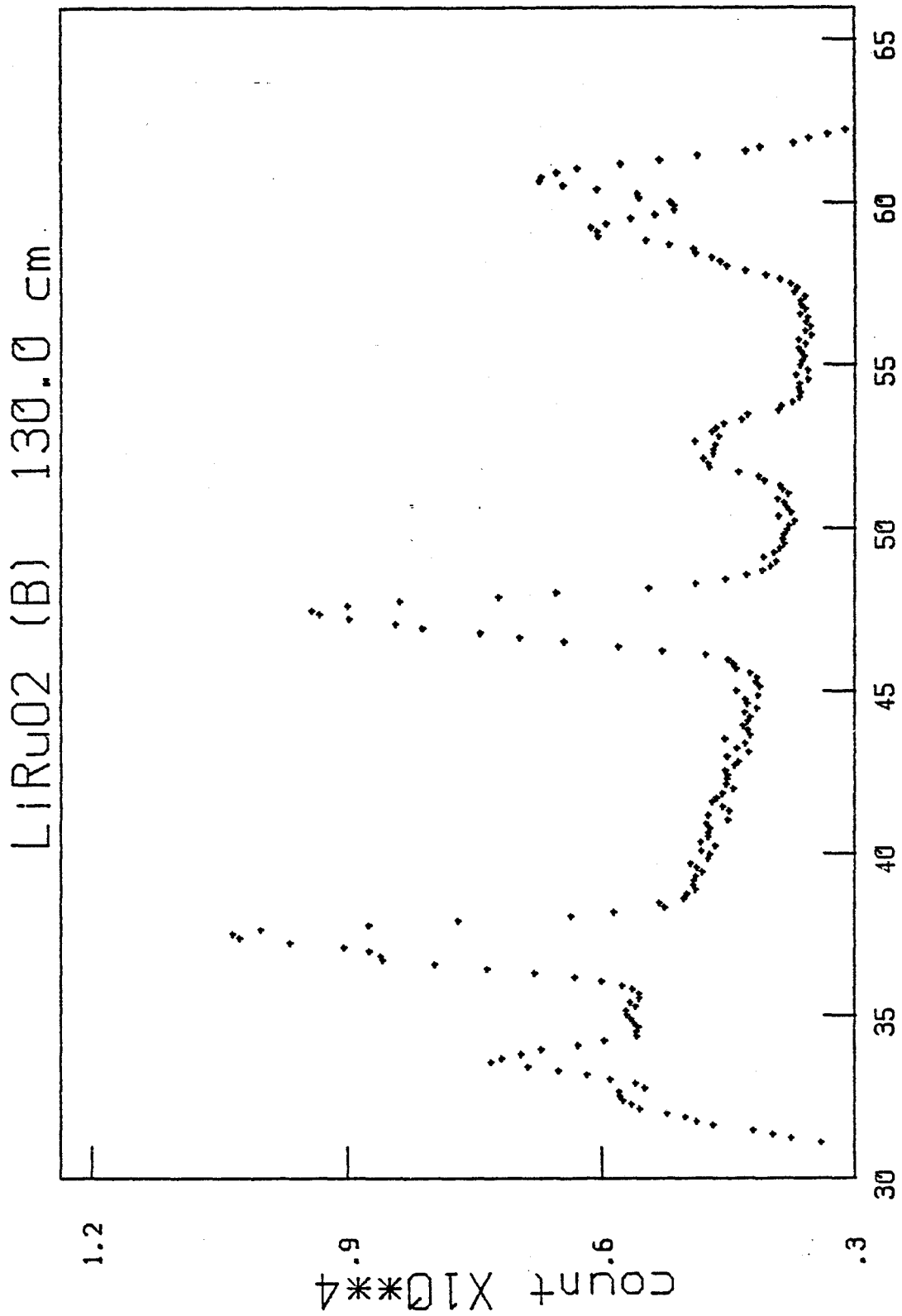
LiRuO2 (B) 130.0 cm
count X10**4
1.2
.9
.6
.3
30
35
40
45
50
55
60
65
2 theta

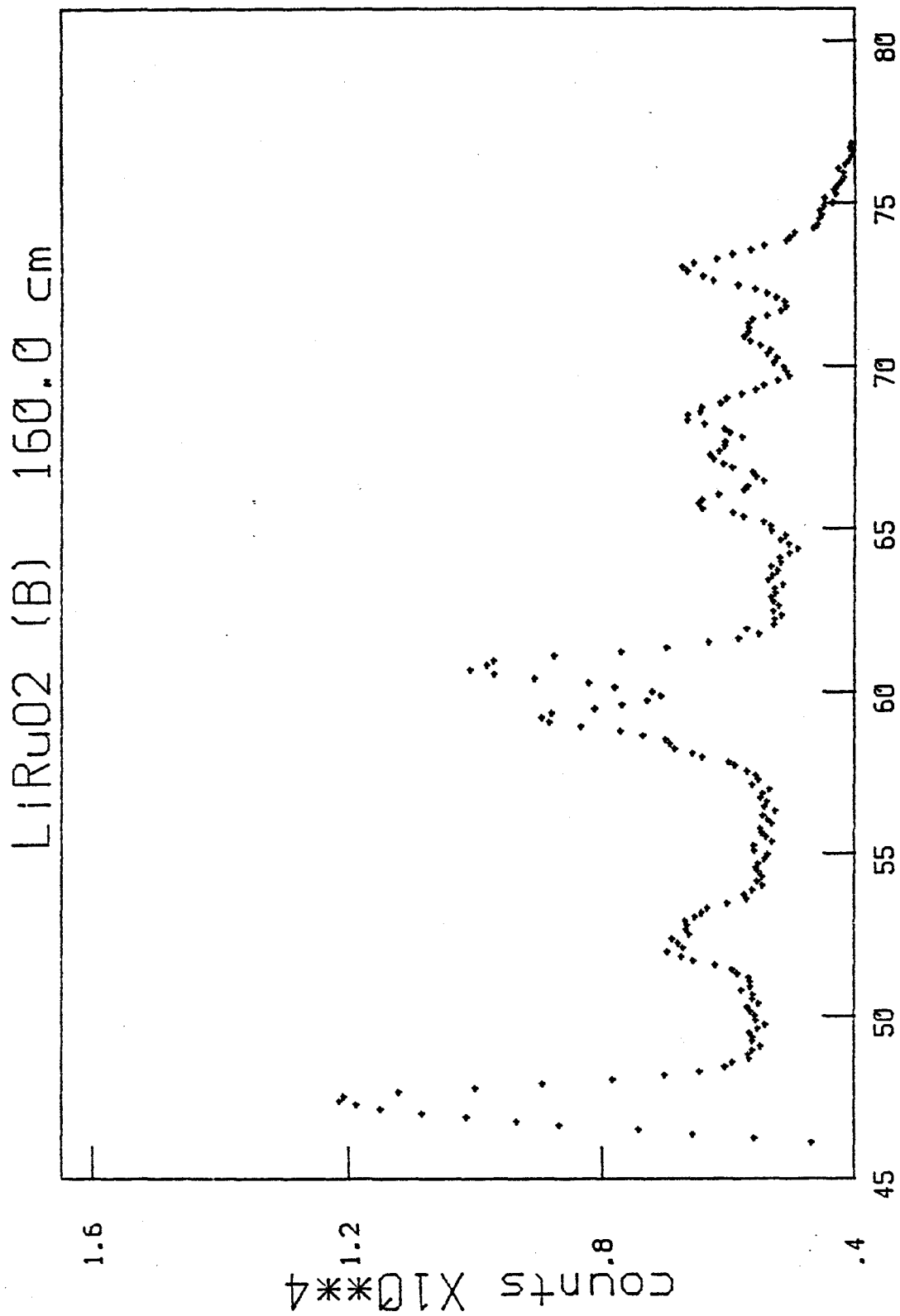
LiRuO2 (B) 160.0 cm
counts X10**4
1.6
1.2
.8
.4
45
50
55
60
65
70
75
80
2 theta

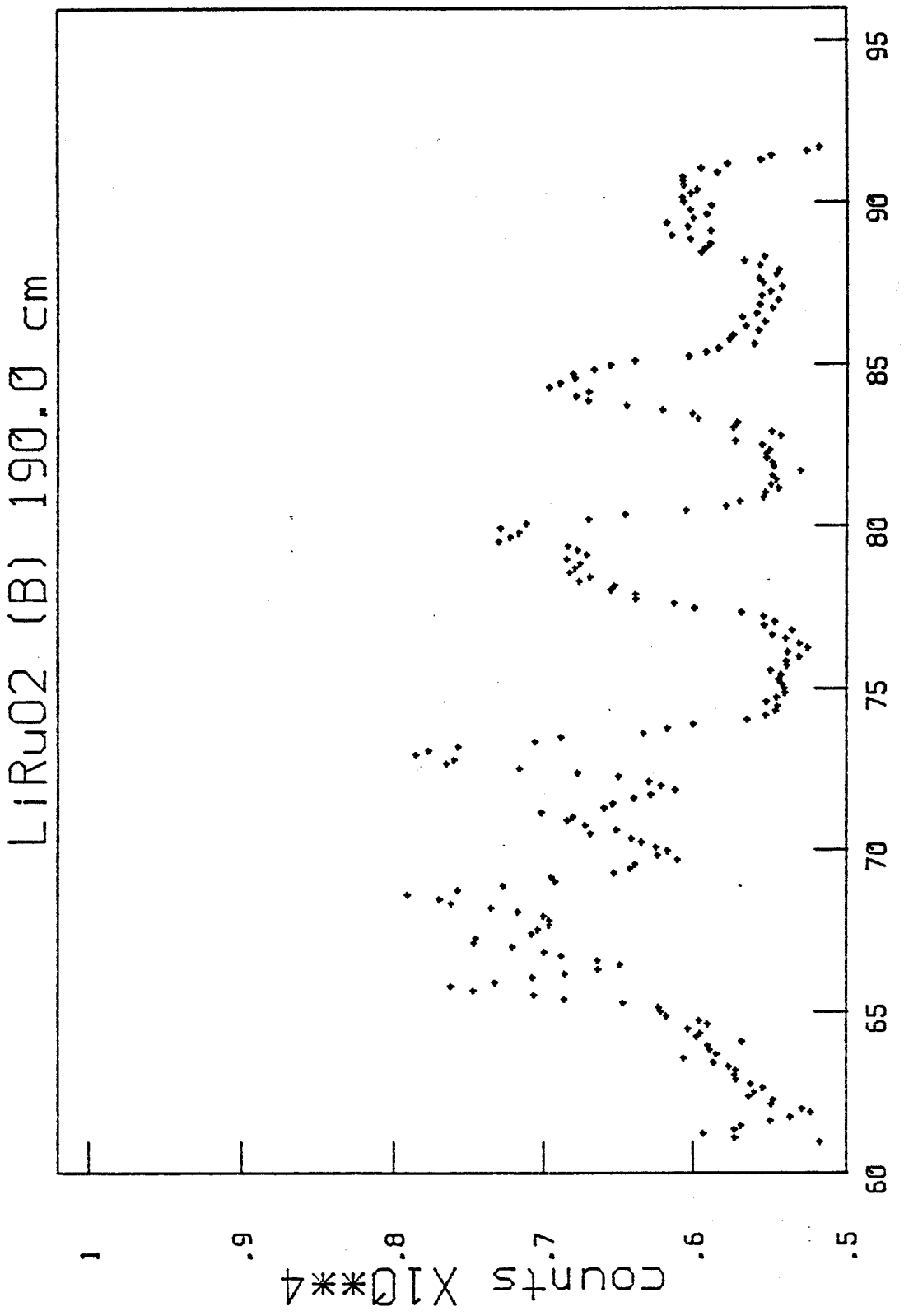
LiRuO2 (B) 190.0 cm
counts X10**4
1
.9
.8
.7
.6
.5
60
65
70
75
80
85
90
95
2 theta

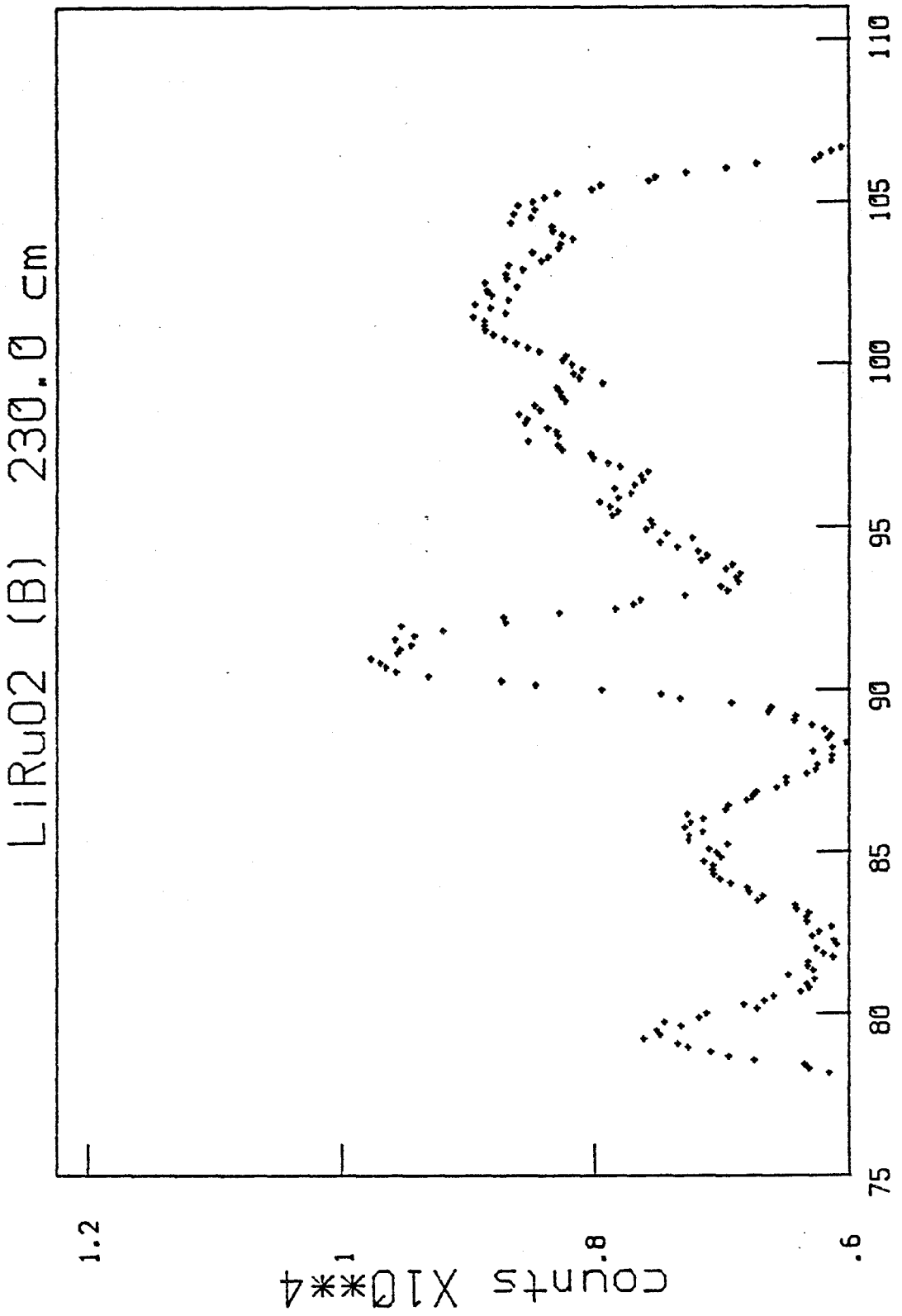
LiRuO2 (B) 230.0 cm
counts X10**4
2 theta (-5.0)
1.2
.9
.6
75
80
85
90
95
100
105
110

Table I.1

Neutron Intensities for $Li_{0.86}RuO_2$

INTENSITIES

H	K	L	THETA	IO	IC	OI/S	SIGMA
			11.39	24159.00	25845.30	-4.062	415.1
			16.06		3179.98		
			16.37		33.14		
				3854.60	3211.52	1.42	454.1
			16.74		11957.11		
			16.81		15.28		
				10670.60	11972.39	-4.45	292.4
			18.08		.02		
			18.30		12621.38		
			18.70		25170.15		
				41332.00	37795.55	8.45	418.8
					10355.98		
					18995.42		
					11985.73		
				41993.00	41333.68	1.85	357.1
				4790.00	5016.03	-1.414	159.8
				5058.40	4863.79	1.072	181.6
*				1.00	.02	9.816	.1
					4670.54		
					14904.44		
				18404.40	18980.38	-2.22	259.5
					5122.49		
					.30		
					7092.22		
					10482.64		
					14.32		
				20986.90	22712.37	-5.33	295.9
				5492.20	6451.52	-3.759	255.2
				5428.60	5956.89	-1.899	267.6
					5982.24		
					4.76		
					3781.50		
				10611.10	9768.44	2.54	331.7
				958.90	.03	3.540	270.9
					1844.32		
					54.76		
					4235.50		
				4233.50	6134.39	-2.33	814.5
					2701.69		
					.01		
					7544.18		
				9835.00	10245.78	-1.16	354.6
					57.29		
					63.60		
					3563.39		
					4703.03		
				8073.60	8387.32	-1.45	216.3
					7771.09		
					9.65		
				7689.40	7781.74	-.44	209.0
					4207.31		
					.14		
					4157.87		
					.11		
				7799.00	8365.23	-.98	576.0
					.10		
					3134.69		
					1914.37		
					5689.93		
					.00		
					1847.99		
				10945.50	12586.69	-3.40	482.0
					1751.61		
					14129.87		
					3462.55		
					2678.36		
					100.58		
					8956.60		
					5541.28		
					.00		
					25.38		
				33183.00	34645.33	-2.74	533.9
					5031.80		
					.03		
					3581.32		
					1639.23		
					47.23		
					3250.82		
					5299.55		
					3191.46		
					29.00		
					5750.39		
					156.58		
					4681.92		
					1518.25		
					1512.60		
					4929.42		
					3027.62		
				52177.00	45646.82	7.76	841.6

***** SUM OF IOBS = .327677E+06***** SUM OF ICALC = .327677E+06 *****

* unobserved reflection.

Table I.2

Neutron Intensities for $Li_{0.87}RuO_2$

INTENSITIES
****

H	K	L	THETA	IO	IC	DI/S	SIGMA
			11.37	6178.39	6481.19	-3.538	85.6
			16.01		624.35		
			16.36		3.49		
			16.67		2647.07		
			16.76		.77		
				2535.41	3275.58	-12.93	57.2
			18.04		13.97		
			18.23		3048.68		
				3026.98	3062.65	-.38	94.8
			18.64	5857.59	5483.15	1.037	341.3
			18.22		2376.55		
			18.31		5144.71		
			18.71		3028.58		
				10028.75	10549.85	-5.18	100.6
			19.91	1103.78	1067.58	.481	75.3
			19.39	1117.65	1085.01	.315	103.6
*			17.88	1.00	12.60	-115.955	.1
			19.36		1272.47		
			19.46		3653.31		
				4414.51	4925.78	-2.12	240.8
			20.03	1154.49	1130.88	.376	62.7
			20.20		1752.38		
			20.28		2081.22		
			20.30		.02		
			20.71		3.93		
				4444.99	3843.56	8.24	73.0
			22.70	1198.96	1672.93	-8.108	58.5
			23.47	1836.10	1453.19	-6.681	62.4
			24.06		1318.43		
			24.29		.08		
			24.32		393.65		
			24.78		15.43		
				1602.03	1727.59	-1.46	86.2
			25.31		188.12		
			25.21		15.13		
			25.45		722.44		
				1477.24	925.69	1.44	383.8
			26.21		7.17		
			26.25		853.47		
			26.36		1594.42		
				2634.91	2455.06	.86	210.2
			28.27		17.39		
			28.49		14.39		
			28.85		1235.67		
			29.21		1241.43		
				2170.69	2509.38	-4.55	74.4
			28.73		1498.38		
					6.88		
			28.99	1659.60	2004.44	-5.44	59.1
			41.79		941.15		
			41.95		23.64		
			42.17		975.87		
			42.52		5.13		
				2243.82	1945.89	3.94	75.7
			44.01		.05		
			44.34		486.31		
			44.72		602.49		
				1110.47	1090.55	.32	62.6
			45.20		1095.32		
			45.44		.02		
			45.86		492.64		
				1516.67	1587.99	-1.07	66.9
			47.21		289.32		
			47.64		3517.72		
			47.97		781.96		
			48.14		491.28		
			48.29		1736.19		
			48.36		913.09		
			48.40		37.66		
			49.05		5.11		
			49.14		2.49		
			49.44		17.36		
				9570.89	7794.79	18.05	93.4

***** SUM OF IOBS = .660849E+05***** SUM OF ICALC = .660849E+05 *****

* unobserved reflection.